IEEE Access
Multidisciplinary | Rapid Review | Open Access Journal

Received December 15, 2020, accepted December 25, 2020, date of publication December 30, 2020,
date of current version January 8, 2021.

Digital Object Identifier 10.1109/ACCESS.2020.3048180

Beamwidth Optimization for Millimeter-Wave V2V Communication Between Neighbor Vehicles in Highway Scenarios

YIJIA FENG, (Member, IEEE), DAZHI HE, YUNFENG GUAN, YIHANG HUANG, YIN XU, (Member, IEEE), AND ZHIYONG CHEN, (Member, IEEE)
School of Electronic Information and Electrical Engineering, Shanghai Jiao Tong University, Shanghai 200240, China

Corresponding author: Yunfeng Guan (yfguan69@sjtu.edu.cn)

This work was supported in part by the National Key Research and Development Project of China under Grant 2018YFB1802202 and Grant 2019YFB1802703, in part by the Shanghai Natural Science Foundation under Grant 19ZR1426600, and in part by the Shanghai Key Laboratory of Digital Media Processing under Grant STCSM 18DZ2270700.

ABSTRACT Millimeter-wave (mmWave) communication is considered to be a promising candidate to enable multi-Gbps data rates in future vehicle-to-everything (V2X) communication. Beam alignment is quite crucial for beam-based mmWave communication and the beam sweeping method is widely adopted for the alignment at present. However, this kind of method will cause large overhead in beam alignment and is inefficient in high mobility environment due to Doppler spread. In this paper, we design an overhead-free vehicular-position-based beam alignment scheme for mmWave V2V communication between neighbor vehicles in highway scenarios. In the proposed beam alignment scheme, the beam is directly steered to the estimated vehicular position without any searching steps in beam training. To avoid beam misalignment caused by localization errors and to maximize transmission throughput, the problem is formulated as a tailored beamwidth optimization problem. A Monte Carlo based Beamwidth Optimization (MCBO) method is developed to divide this optimization into two phases and solve this problem statistically. Simulation results demonstrate that, comparing to the widely-adopted beam-sweeping based beam alignment schemes, the proposed vehicular-position-based overhead-free beam alignment scheme with MCBO method can provide significant throughput improvements in general car-following scenarios on the highway.

INDEX TERMS Vehicle-to-vehicle communication, millimeter-wave communication, beam alignment, beamwidth optimization.

I. INTRODUCTION

OVER the years, to enhance traffic safety and enable driving automation, there is a considerable growth of embedded sensors inside vehicles [1]. By sharing the local sensor data with surrounding environment via vehicle-to-everything (V2X) communication, vehicles can collectively perceive the environment. For instance, Samsung developed a collective perception application [2] which provides the vehicle behind a truck with a see-through vision of the on-coming traffic situation ahead of the truck via vehicle-to-vehicle (V2V) communication. As suggested in [3], the collective perception applications extend the perception range of vehicles beyond their immediate field of view, enhancing traffic safety and efficiency. According to 3GPP TS 22.186 [4] and 3GPP TR 22.886 [5], the delivery for collective perception of environment requires data rates on the order of Gbps. Unfortunately, none of the existing V2X communication standards can support such Gbps-level data rates. For the Dedicated Short Range Communication (DSRC), the maximum data rate is only 27 Mbps [6]. Long Term Evolution (LTE)-V2X can achieve up to 80 Mbps for downlink and 20 Mbps for uplink [7]. Facing this challenge, thanks to the ultra-wide GHz spectrum at the millimeter-wave (mmWave) frequency band, the mmWave communication becomes a promising candidate to fulfill this transmission requirement [8].

However, due to the short wavelength, mmWave communication suffers from severe path loss. Additionally, the inherent

The associate editor coordinating the review of this manuscript and approving it for publication was Cunhua Pan.

propagation characteristics also make the mmWave transmission sensitive to blockage, rainfall, and atmospheric absorption, which brings large attenuation [9]. Thus, directional beamforming is often utilized in mmWave communication system to deal with these impairments [10].

To fully exploit the directivity gain, fine beam alignment is crucial for the transmitter (Tx) and receiver (Rx) beams. In current mmWave communication standards IEEE 802.11ad [11] and IEEE 802.15.3c [12], two-stage beam training procedures are designed for beam alignment. In the first phase, a coarse grained sector-level sweep is performed, then in the second phase, a fine grained beam-level sweep is implemented [13], [14]. The exhaustive search over all possible transmission and reception directions is utilized in both phases, which induces a tradeoff between directivity gain and beam alignment overhead in the beamwidth optimization. This is because, although narrower beam has a larger beamforming gain, it increases the beam candidates that need to be searched, thus raising the overhead in beam alignment and lessening the time for data transmission [15].

Therefore, with the tradeoff between the directivity gain and beam alignment overhead, optimizing the beamwidth in the beam-sweeping-based beam alignment scheme attracts considerable attention of researchers. The research in [16] provides a unifying framework which brings beam-searching and transmission scheduling together, then addresses a joint beamwidth optimization and power allocation problem to maximize effective network throughput. On the basis of this unifying framework, many studies [17]–[22] scrutinize the tradeoff to improve transmission performance. In particular, in [20], the aforementioned tradeoff and framework are extended to the vehicular environment with the proposed radio resource management scheme based on matching theory and swarm intelligence. Then, in [21], a decentralized vehicle association algorithm is developed with the consideration of the above fundamental beamwidth tradeoff to enhance content dissemination in mmWave V2V communication. Furthermore, different from the suboptimal interference-estimation-based algorithms in [16], a deep reinforcement learning approach is recently proposed to solve the joint beamwidth and power control problem in [22].

However, as first suggested in [23], the above widely-adopted beam-sweeping-based beam alignment is inefficient for high mobility environment because of the Doppler spread. Hence, a beam switching scheme leveraging the position information of the high speed train is designed in [23] for efficient beam alignment. Moreover, a fundamental beamwidth design tradeoff is revealed in [23] that wider beams suffer from insufficient power but narrower beams are more sensitive to position error. Accordingly, there arises another beam alignment research direction for vehicle-to-infrastructure (V2I) mmWave communication where beam sweeping can be much diminished or even omitted with estimated position information [24]–[31]. In [24], the study investigates the beam design to maximize the data rate in a beam-switching-based V2I system, where the vehicular position is predicted by the estimated speed with Gaussian error. In [25] and [26], similar overhead-free beam training mechanisms are exploited with the estimated vehicular position and motion information in V2I communication. In [27], taking into account the position uncertainty of high mobility users, a joint adaptive beam-frequency allocation algorithm is developed to balance the tradeoff between system performance and robustness to uncertainty. The study in [28] derives a close-form expression of the optimal receive beamwidth in V2I downlink transmissions. Accordingly, the study in [29] answers the question of when the beam should be realigned in such V2I communication system. Then, in [30], a mobility-aware subband and beam resource allocation scheme is proposed for mmWave-based subband-beam massive MIMO system, which can also be applied in V2I communication. Moreover, in [31], an IEEE 802.11ad MAC configuration is proposed to embed the radar functionality within the standards-compliant operations. Different from the above overhead-free beam alignment schemes, this mechanism uses the same band (IEEE 802.11ad) to obtain the vehicular positions and thus cuts down the time needed for classical beam training in V2I communication system.

Besides being applied in V2I communication, the position information is also utilized in V2V communication. In [32], a directional mmWave transmission scheme with vehicular position information is proposed to minimize energy consumption. However, the position error is modeled to be restricted in a circle of perfect symmetry, which limits its adaptability in high mobility environment.

From the above literature survey, considering the deficiency of the widely-adopted beam-sweeping-based beam alignment in high mobility environment, applying overhead-free beam alignment with estimated vehicular positions and optimizing the beamwidths to maximize the transmission rate in the system is appealing to V2X communication in the upcoming autonomous vehicle era. To the best knowledge of authors, this mechanism has only been proposed for V2I communication. Therefore, motivated by the aforementioned works, this paper studies an overhead-free vehicular-position-based beam alignment scheme and the corresponding beamwidth optimization methods to maximize the system throughput for mmWave V2V communication between neighbor vehicles in the highway scenario. Distinct from V2I scenario, both Txs and Rxs are of high mobility and with estimated positions in V2V scenario, which brings new research challenges. The proposed scheme can be applied in the aforementioned collective perception applications in highway scenario to provide enhanced throughput performance for better traffic safety and efficiency. The main contributions of this paper can be summarized as the following points:

- A vehicular-position-based overhead-free beam alignment scheme is proposed for V2V communication between neighbor vehicles in the highway scenario in this paper. In the proposed beam alignment scheme, with the position information gathered by localization tech-

nologies, the beam is directly steered to the estimated vehicular position without any searching steps in beam training.

- Given the uncertainty of vehicular real positions caused by localization errors, a tailored beamwidth optimization problem is formulated to maximize the sum of the average transmission throughput in the nearby regions of the Rxs in the system. Then, due to the intractability of uncertain real vehicular positions, we develop a Monte Carlo based Beamwidth Optimization (MCBO) method to solve this problem.
- In the MCBO method, the optimization is divided into two phases: 1) Under the assumption that the real positions of Txs and Rxs are certain, the problem is first simplified as a conventional resource allocation problem, which can be proven as a standard difference of two convex functions (D.C.) problem and handled by convex optimization approaches. 2) After solving the beamwidth optimization problem with assumed certain real positions, considering the uncertainty of vehicular real positions, Monte Carlo method is utilized to simulate the real positions of Txs and Rxs. Accordingly, optimal beamwidth finding algorithms are developed to find the optimal beamwidths with small computation complexity.
- Simulation results are presented to validate the capability of the proposed overhead-free beam alignment scheme and the corresponding beamwidth optimization method. From the comparisons between the proposed scheme and the existing schemes in [16] and [22], which are inherited from the existing IEEE mmWave standards, we can see the proposed scheme can provide significant performance improvements in general car-following scenarios on the highway.

The remainder of this paper is organized as follows. First, Section II introduces the system model and the beamwidth optimization problem formulation. In Section III, MCBO method is developed to solve the beamwidth optimization problem. Furthermore, in Section IV, simulation results are presented to validate the feasibility of the proposed beam alignment scheme and the corresponding beamwidth optimization method. Finally, Section V concludes this paper.

II. SYSTEM MODEL AND PROBLEM FORMULATION

In this paper, we focus on the mmWave V2V communication between neighbor vehicles running in the same direction on the highway scenario. In this scenario, information is delivered from front vehicles to rear vehicles. Since vehicles run at a very high speed, the safe inter-vehicle space should be kept as several tens of meters. For instance, when the velocities of both vehicles are 100 km/h and the headway is 3 s in the car-following scenario, the inter-vehicle distance should be around 80 m, which indicates the communication distance in this scenario is generally larger than that in the common mmWave communication cases. It is intuitive to leverage thin beam to compensate the pathloss of long communication distance in mmWave communication. However, in the widely-adopted beam-sweeping-based beam alignment scheme, thin beam will lead to large overhead. Moreover, due to Doppler spread, thin beam will make the transmission inefficient in high mobility environment. Hence, based on mmWave communication and analog beamforming technology, we propose a new vehicular-position-based overhead-free beam alignment scheme for mmWave V2V communication between neighbor vehicles in the highway scenario.

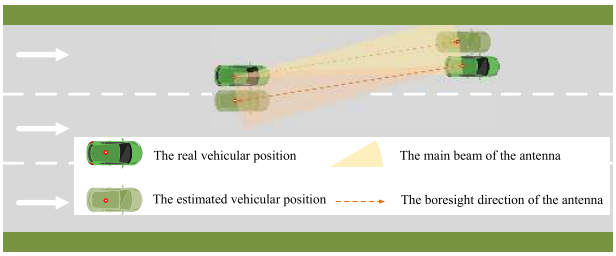

FIGURE 1. The schematic of the proposed overhead-free beam alignment scheme.

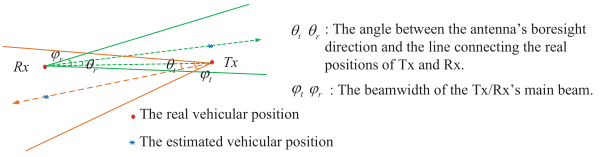

FIGURE 2. The geometric schematic of the proposed overhead-free beam alignment scheme.

A. SCHEMATIC MODEL OF THE PROPOSED OVERHEAD-FREE BEAM ALIGNMENT SCHEME

The schematic of the proposed overhead-free beam alignment scheme is illustrated in Fig. 1. In Fig. 1, vehicles run on a multi-lane highway segment, which is modeled as a two-dimension plane. Then, vehicles are assumed to be able to obtain the position information of other vehicles, which will be detailed explained in Section II-D. Next, with the position information, the Tx and Rx vehicles can directly align their main beam to the position of their partner without any searching steps, indicating this beam alignment scheme is overhead-free.

Fig. 2 is the more specific schematic abstracting from Fig. 1, showing the geometric description of the proposed overhead-free beam alignment scheme. In Fig. 2, the red dots denote the real vehicular positions and the blue asterisks refer to the estimated vehicular positions. The arrow implies the boresight direction of the antenna, which starts from the real position of a vehicle and points at the estimated position of another vehicle. Accordingly, θ_t and θ_r are the angles between the antennas' boresight directions and the line connecting the real positions of Tx and Rx, indicating the alignment angle errors. Furthermore, φ_t and φ_r represent the beamwidths of Tx and Rx.

B. CHANNEL MODEL

Considering highway is an open space without many obstructions and in order to make the channel model tractable, we simplify the model by ignoring the multi-path propagations, which may be caused by the presence of other vehicles in the neighbor lanes. Then, in accordance to 3GPP TR 37.885 [33], the V2V sidelink channel can be classified into three states, including LOS, NLOS (blocked by buildings), and NLOSv (blocked by vehicles). Since we study the V2V communication of adjacent vehicles on the highway, there is a dominant LOS path between the Tx vehicle and its target Rx vehicle. Then, for the channel between the interfering Tx vehicle and the target Rx vehicle, depending on whether the LOS path is blocked by a vehicle, it can be categorized as LOS channel or NLOSv channel. In addition, without loss of generality, the vehicular antenna is assumed to be located at the car roof center, and the rear or front antenna is not considered in this paper.

For both LOS and NLOSv cases, the log-distance pathloss model of highway cases described in 3GPP TR 37.885 [33] is adopted for channel modeling in this paper. According to the channel model, the propagation loss $L^{i,j}$ between Tx i and Rx j is calculated as

$$L^{i,j} = 32.4 + 20\log_{10}D^{i,j} + 20\log_{10}f_c, \tag{1}$$

where $D^{i,j}$ denotes the distance between Tx i and Rx j in meters, and f_c denotes the center frequency in GHz. For NLOSv cases, additional vehicle blockage loss L_{NLOSv} is added as

$$L_{NLOSv} = \max(0\ \text{dB}, A_{NLOSv}), \tag{2}$$

where A_{NLOSv} is a log-normal random variable. The mean of A_{NLOSv} equals $[5 + \max(0, 15\log_{10}(D^{i,j}) - 41)]$ dB and the standard deviation of A_{NLOSv} equals 4 dB.

C. ANTENNA GAIN MODEL

For the sake of mathematical tractability, a widely used antenna gain piecewise model [16], [20], [34], [35] is adopted in this paper as following,

$$G_\gamma(\theta_\gamma{}^{i,j}, \varphi_\gamma^{i,j}) = \begin{cases} \dfrac{2\pi - (2\pi - \varphi_\gamma^{i,j})g}{\varphi_\gamma^{i,j}}, & \text{if } |\theta_\gamma{}^{i,j}| \le \dfrac{\varphi_\gamma^{i,j}}{2}, \\ g, & \text{otherwise}, \end{cases} \tag{3}$$

where the subscript $\gamma \in \{t, r\}$, t represents Tx and r represents Rx. The angle between the antenna boresight direction of Tx i and the beam steering direction from Tx i to Rx j is denoted as $\theta_t^{i,j}$, which is also regarded as the alignment angle error illustrated in Fig. 2. Likewise, we have $\theta_r^{i,j}$. $\varphi_\gamma^{i,j}$ stands for the beamwidth of Tx i or Rx j. Besides, the beamwidth of Tx i can also be denoted as φ_t^i, and the beamwidth of Rx j can be denoted as φ_r^j. g is a small constant indicating the side lobe gain of the antenna. $0 \le g \ll 1$ guarantees most of the antenna power is dominated by its main lobe.

D. INACCURATE POSITIONING

First, we assume that vehicles are able to get their relative positions to other vehicles via some other advanced sensing techniques (eg. LiDAR, Radar, and ultrasonic-based techniques) or Global Navigation Satellite System (GNSS). Then, vehicles broadcast their basic safety messages (BSM) through some lower band V2X communication. Here, the BSM includes their relative positions to other vehicles, localization accuracy, velocity, and acceleration information. Additionally, in case of the saturated channel caused by periodic transmission of BSM, the strategies proposed in [36] can be adopted in this scenario to control the channel load and ensure high reception rate.

We generally assume the position error of these different localization techniques as the Gaussian-distributed position estimation model and the position error for each vehicle is independent of each other. Motivated by the Central Limit Theorem, although the Gaussian assumption may not be absolutely valid, the large number of small, independent error sources in a navigation system results in error distributions that can be accurately approximated as Gaussian [37].

Then, denote (x, y) as a real vehicular position at a given moment, denote $(\hat{x}, \hat{y})$ as an estimated vehicular position, and the estimated vehicular position coordinates $\hat{X}$ and $\hat{Y}$ are assumed to follow Gaussian distributions $\hat{X} \sim N(x, \sigma_X^2)$ and $\hat{Y} \sim N(y, \sigma_Y^2)$ respectively. σ_X^2 and σ_Y^2 are the variances of the localization technology's Gaussian distributions.

Furthermore, given the mobility of vehicles, after a short period t, the vehicular coordinates can be updated as

$$\begin{aligned} x_t &= x + v_x t, \\ y_t &= y + v_y t. \end{aligned} \tag{4}$$

Due to the inaccuracy of velocity approximation caused by acceleration or deceleration in the short period, vehicular velocities V_x and V_y in X-axis and Y-axis are also assumed to follow Gaussian distributions $V_x \sim N(v_x, \sigma_{V_x}^2)$ and $V_y \sim N(v_y, \sigma_{V_y}^2)$.

Thus, the estimated position coordinates $\hat{X}_t$ and $\hat{Y}_t$ of the mobile vehicle, which update after a short period t, still follow Gaussian distributions as

$$\begin{aligned} \hat{X}_t &\sim N(x + v_x t, \sigma_X^2 + t^2\sigma_{V_x}^2), \\ \hat{Y}_t &\sim N(y + v_y t, \sigma_Y^2 + t^2\sigma_{V_y}^2). \end{aligned} \tag{5}$$

Therefore, the position accuracy of the mobile vehicle is related to the initial localization error, the approximated velocity error, and the location refresh period.

However, in reality, vehicles can only obtain the estimated position information of other vehicles while never know their real positions. Thus, in the following analysis, distinct from the above description, the real vehicular position coordinates X and Y turn to be the random variables that follow Gaussian distributions $X \sim N(\hat{x}, \sigma_X^2)$ and $Y \sim N(\hat{y}, \sigma_Y^2)$ respectively. Similarly, the real position coordinates X_t and Y_t of a mobile

vehicle follow Gaussian distributions demonstrated as

$$X_t \sim N(\hat{x} + v_x t, \sigma_X^2 + t^2\sigma_{V_x}^2),$$
$$Y_t \sim N(\hat{y} + v_y t, \sigma_Y^2 + t^2\sigma_{V_y}^2). \quad (6)$$

It is worth noting that, the Gaussian-distributed position estimation model is an indicator of position error and used for analytical purpose. If the position error of a specific localization technique has a different realistic distribution, it can be directly substituted into the proposed MCBO method, which enhances the adaptability of the method.

E. TRANSMISSION RATE

In this paper, suppose there are N independent V2V communication links running on the highway segment in the system, the transmitting power p_t and bandwidth B are supposed to be same for each vehicular link. Therefore, the signal to interference plus noise ratio (SINR) of the i^{th} vehicular link is calculated as

$$SINR_i(\boldsymbol{\theta}_i, \boldsymbol{\varphi}_i) = \frac{p_t L^{i,i} G_t(\theta_t^{i,i}, \varphi_t^i) G_r(\theta_r^{i,i}, \varphi_r^i)}{N_0 B + \sum_{k\neq i}^{N} p_t L^{k,i} G_t(\theta_t^{k,i}, \varphi_t^k) G_r(\theta_r^{k,i}, \varphi_r^i)}. \quad (7)$$

Here, N_0 is the Gaussian noise density, N is the number of the vehicular links in the system, $\boldsymbol{\theta}_i = (\theta_t^{1,i}, \cdots, \theta_t^{N,i}, \theta_r^{1,i}, \cdots, \theta_r^{N,i})$ denotes the alignment angle error vector, and $\boldsymbol{\varphi}_i = (\varphi_t^1, \cdots, \varphi_t^N, \varphi_r^i)$ denotes the $(N+1)$-dimensional beamwidth vector. Thus, the transmission rate of the i^{th} vehicular link can be calculated as

$$r_i(\boldsymbol{\theta}_i, \boldsymbol{\varphi}_i) = B\log_2(1 + SINR_i(\boldsymbol{\theta}_i, \boldsymbol{\varphi}_i)). \quad (8)$$

F. PROBLEM STATEMENT

In the proposed overhead-free beam alignment scheme, as demonstrated in Fig. 2, only under the circumstances of $|\theta_\gamma| \leq \frac{\varphi_\gamma}{2}$ ($\gamma \in \{t, r\}$), can the real vehicular position be covered by the main beam. Hence, the beamwidth optimization problem in the proposed overhead-free beam alignment scheme comes with a fundamental tradeoff: if the beam is too wide, the antenna gain will degrade, while if the beam is too narrow, the real position of the target vehicle may not be covered by the main beam and misalignment may happen.

Based on the above tradeoff, our goal is to find the optimal beamwidths that can both maximize transmission throughput and avoid beam misalignment in the system. To avoid beam misalignment, the problem is formulated to maximize the sum of the average throughput in the Rxs' estimated position coordinates' nearby regions, rather than simply maximizing the sum throughput of the Rxs. Thus, the formulated problem can be expressed as

$$\max_{\boldsymbol{\varphi}_t, \boldsymbol{\varphi}_r} \sum_{i=1}^{N} \mathop{\mathbb{E}}_{\boldsymbol{X},\boldsymbol{Y}} [B \cdot \log_2(1 + SINR_i(\boldsymbol{\theta}_i, \boldsymbol{\varphi}_i))] \quad (9a)$$
$$\text{s.t. } 0 < \varphi_t^i \leq \psi_t^i, \quad \forall i \quad (9b)$$
$$0 < \varphi_r^i \leq \psi_r^i, \quad \forall i. \quad (9c)$$

In (9), $\boldsymbol{\varphi}_t$ and $\boldsymbol{\varphi}_r$ are the beamwidth vectors, where $\boldsymbol{\varphi}_t = (\varphi_t^1, \cdots, \varphi_t^N)$ and $\boldsymbol{\varphi}_r = (\varphi_r^1, \cdots, \varphi_r^N)$. $\boldsymbol{X}$ and $\boldsymbol{Y}$ are random variable sets containing the real vehicular position coordinates of all the Txs and Rxs. $\boldsymbol{X}$ and $\boldsymbol{Y}$ can also be replaced by the random variable sets $\boldsymbol{X}_t$ and $\boldsymbol{Y}_t$ to calculate the average throughput with vehicular mobility. For description simplicity, Section III solves the problem based on $\boldsymbol{X}$ and $\boldsymbol{Y}$. The extension problem based on $\boldsymbol{X}_t$ and $\boldsymbol{Y}_t$ has identical solutions. Then, ψ_t^i and ψ_r^i stand for the sector widths of the Tx and Rx in the i^{th} vehicular link. (9b) and (9c) indicate the beamwidths of the Tx and Rx in the i^{th} vehicular link should be adjusted within their sector widths.

III. PROPOSED MONTE CARLO BASED BEAMWIDTH OPTIMIZATION METHOD

In this section, we propose the MCBO method to tackle the problem in (9). We first analyze the problem and explain the difficulty of solving it in Section III-A. After that, we elaborate on the two phases of the MCBO method in Section III-B.

A. PROBLEM ANALYSIS

To solve the optimization problem in (9), we first exchange the order of the sum and the mathematical expectation in (9a). Then, the optimization problem in (9) can be rewritten as the following equivalent form

$$\max_{\boldsymbol{\varphi}_t, \boldsymbol{\varphi}_r} \iint_{(\boldsymbol{x},\boldsymbol{y})\in\Omega_{(\hat{\boldsymbol{x}},\hat{\boldsymbol{y}})}} \left(\sum_{i=1}^{N} [B \cdot \log_2(1 + SINR_i(\boldsymbol{\theta}_i, \boldsymbol{\varphi}_i))] \right) f(\boldsymbol{x}, \boldsymbol{y}) d\boldsymbol{x} d\boldsymbol{y},$$
$$\text{s.t. (9b), (9c)}, \quad (10)$$

where $\boldsymbol{x}$ and $\boldsymbol{y}$ are 2N-dimensional position coordinate vectors representing the real position coordinates of all the Txs and Rxs, expressed as

$$\boldsymbol{x} = (x_t^1, \cdots, x_t^N, x_r^1, \cdots, x_r^N),$$
$$\boldsymbol{y} = (y_t^1, \cdots, y_t^N, y_r^1, \cdots, y_r^N). \quad (11)$$

Considering the three-sigma (3σ) rule of Gaussian distribution, which suggests the probability that the statistical data lie out of the three standard deviations from the mean is less than 0.3%, the real vehicular position coordinate has the most probability lying in the 3σ domain of its estimated position. Thus, $\Omega_{(\hat{\boldsymbol{x}},\hat{\boldsymbol{y}})}$ represents the 3σ domain of $(\hat{\boldsymbol{x}}, \hat{\boldsymbol{y}})$, implying the nearby regions of all the Txs' and the Rxs' estimated positions.

Then, in the optimization object in (10), $f(\boldsymbol{x}, \boldsymbol{y})$ is the joint Gaussian probability density function of $\boldsymbol{x}$ and $\boldsymbol{y}$ given by

$$f(\boldsymbol{x}, \boldsymbol{y}) = \frac{1}{\sqrt{(2\pi)^{4N}\det(\boldsymbol{\Lambda})}} \exp\left[-\frac{1}{2} (\boldsymbol{p} - \boldsymbol{\mu})^T \boldsymbol{\Lambda}^{-1} (\boldsymbol{p} - \boldsymbol{\mu}) \right], \quad (12)$$

where $\boldsymbol{p}$ is the integrated vector of $\boldsymbol{x}$ and $\boldsymbol{y}$, expressed as

$$\boldsymbol{p} = ([\boldsymbol{x}, \boldsymbol{y}]) = (x_t^1, \cdots, x_t^N, x_r^1, \cdots, x_r^N, y_t^1, \cdots, y_t^N, y_r^1, \cdots, y_r^N), \quad (13)$$

$\boldsymbol{\mu}$ denotes the mathematical expectation vector of $\boldsymbol{x}$ and $\boldsymbol{y}$, expressed as

$$\boldsymbol{\mu} = (\hat{x}_t^1, \cdots, \hat{x}_t^N, \hat{x}_r^1, \cdots, \hat{x}_r^N, \hat{y}_t^1, \cdots, \hat{y}_t^N, \hat{y}_r^1, \cdots, \hat{y}_r^N), \tag{14}$$

$\boldsymbol{\Lambda}$ represents the corresponding covariance matrix, expressed as

$$\boldsymbol{\Lambda} = diag(\sigma_{X,t}^{1\ 2}, \cdots, \sigma_{X,t}^{N\ 2}, \sigma_{X,r}^{1\ 2}, \cdots, \sigma_{X,r}^{N\ 2}, \sigma_{Y,t}^{1\ 2}, \cdots, \sigma_{Y,t}^{N\ 2}, \sigma_{Y,r}^{1\ 2}, \cdots, \sigma_{Y,r}^{N\ 2}). \tag{15}$$

Because the position error for each vehicle is assumed to be independent of each other, the covariance matrix $\boldsymbol{\Lambda}$ is a diagonal matrix, whose diagonal elements are the variances of the position coordinates. Furthermore, it should be noted that, since vehicles may use different localization technologies to obtain their own relative positions to other vehicles, the elements in $\boldsymbol{\Lambda}$ may have different values. For instance, in a single link scenario, the localization errors of Tx and Rx may be different. Therefore, such beamwidth optimization between Tx and Rx is not reciprocal and the beamwidths should be optimized for both sides.

As described above, the optimization object in problem (10) is of high dimension. The piecewise antenna gain model in (3) makes the numerator and denominator of $SINR_i(\boldsymbol{\theta}_i, \boldsymbol{\varphi}_i)$ in (7) become nonconvex functions. Then, since the numerator and denominator of $SINR_i(\boldsymbol{\theta}_i, \boldsymbol{\varphi}_i)$ are both affected by φ_r^i, the numerator and denominator of $SINR_i(\boldsymbol{\theta}_i, \boldsymbol{\varphi}_i)$ are not independent of each other. Moreover, since the $SINR$s of all the communication links are affected by φ_t^i $(\forall i)$, the $SINR$s of all the communication links are not independent of each other. Hence, given the reasons above, the problem (10) is challenging to handle. In our previous work [38], a discretization-based beamwidth optimization method is developed to solve this problem by discretizing the integral into several small grid zones to approximate the object of the problem. However, in this discretization-based beamwidth optimization method, mere increment of discretization zone precision will lead to dramatic increase of computation. Then, with the increment of the system scale, the computation complexity will be exponential. Hence, in order to reduce computation complexity, a new MCBO method is proposed to solve the problem (10) in this paper.

B. MONTE CARLO BASED BEAMWIDTH OPTIMIZATION

To solve the problem (10), we first scrutinize the optimization object. Herein, the probability density function $f(\boldsymbol{x}, \boldsymbol{y})$ does not contain the optimization variables $\boldsymbol{\varphi}_t$ and $\boldsymbol{\varphi}_r$, which indicates with the given $(\boldsymbol{x}, \boldsymbol{y})$, $f(\boldsymbol{x}, \boldsymbol{y})$ can be recognized as a constant to $\boldsymbol{\varphi}_t$ and $\boldsymbol{\varphi}_r$. Therefore, we can first set the $f(\boldsymbol{x}, \boldsymbol{y})$ aside and solve the problem without regard to $f(\boldsymbol{x}, \boldsymbol{y})$, which can be considered as optimizing the beamwidths when the real vehicular positions are assumed to be certain. Then, considering $f(\boldsymbol{x}, \boldsymbol{y})$ is a nonintegrable function of high dimension, Monte Carlo method is utilized to simulate $f(\boldsymbol{x}, \boldsymbol{y})$ and solve the problem (10). Thus, the solution to the optimization problem (10) is divided into the following two phases in our proposed MCBO method.

1) BEAMWIDTH OPTIMIZATION WITH CERTAIN REAL POSITIONS

In this subsection, the probability density function $f(\boldsymbol{x}, \boldsymbol{y})$ in problem (10) is firstly set aside and the real vehicular positions are assumed to be certain, which transfers the problem (10) into problem (16), as shown at the bottom of the page. Then, denote the alignment angle error matrix $\boldsymbol{\theta}_\gamma$ as

$$\boldsymbol{\theta}_\gamma = \begin{pmatrix} \theta_\gamma^{1,1} & \cdots & \theta_\gamma^{1,N} \\ \vdots & \ddots & \vdots \\ \theta_\gamma^{N,1} & \cdots & \theta_\gamma^{N,N} \end{pmatrix}, \quad \gamma \in \{t, r\}. \tag{17}$$

With the certain positions of Txs and Rxs, the alignment angle error matrix $\boldsymbol{\theta}_\gamma (\gamma \in \{t, r\})$ is fixed. Then, the antenna gain in problem (16) becomes the function only depending on the beamwidth $\boldsymbol{\varphi}$, expressed as

$$G_\gamma^{\ i,j}(\varphi_\gamma^{i,j}) = \begin{cases} \dfrac{2\pi - (2\pi - \varphi_\gamma^{i,j})g}{\varphi_\gamma^{i,j}}, & \text{if } \varphi_\gamma^{i,j} \geq 2|\theta_\gamma^{\ i,j}|, \\ g, & \text{otherwise,} \end{cases} \quad \gamma \in \{t, r\}. \tag{18}$$

Accordingly, the problem (16) can be solved by convex optimization approaches as follows.

First, the problem (16) is equivalent to

$$\max_{\boldsymbol{\varphi}_t, \boldsymbol{\varphi}_r} \sum_{i=1}^{N} B \cdot \log_2 \left(N_0 B + \sum_{k=1}^{N} p_t L^{k,i} G_t^{k,i}(\varphi_t^k) G_r^{k,i}(\varphi_r^i) \right) - \sum_{i=1}^{N} B \cdot \log_2 \left(N_0 B + \sum_{k=1, k\neq i}^{N} p_t L^{k,i} G_t^{k,i}(\varphi_t^k) G_r^{k,i}(\varphi_r^i) \right) \quad \text{s.t. (9b), (9c).} \tag{19}$$

In the optimization object of problem (19), the two terms can be denoted as

$$h(\boldsymbol{\varphi}_t, \boldsymbol{\varphi}_r) = \sum_{i=1}^{N} B \log_2 \left(N_0 B + \sum_{k=1}^{N} p_t L^{k,i} G_t^{k,i}(\varphi_t^k) G_r^{k,i}(\varphi_r^i) \right), \tag{20}$$

$$\max_{\boldsymbol{\varphi}_t, \boldsymbol{\varphi}_r} \sum_{i=1}^{N} B \cdot \log_2 \left(1 + \frac{p_t L^{i,i} G_t^{i,i}(\varphi_t^i) G_r^{i,i}(\varphi_r^i)}{N_0 B + \sum_{k\neq i}^{N} p_t L^{k,i} G_t^{k,i}(\varphi_t^k) G_r^{k,i}(\varphi_r^i)} \right) \quad \text{s.t.} \quad \text{(9b), (9c),} \tag{16}$$

$$g(\boldsymbol{\varphi}_t, \boldsymbol{\varphi}_r) = \sum_{i=1}^{N} B \log_2 \left(N_0 B + \sum_{\substack{k=1 \\ k \neq i}}^{N} p_t L^{k,i} G_t^{k,i}(\varphi_t^k) G_r^{k,i}(\varphi_r^i) \right). \tag{21}$$

More specifically, the logarithmic function in each term in function $h(\boldsymbol{\varphi}_t, \boldsymbol{\varphi}_r)$ and $g(\boldsymbol{\varphi}_t, \boldsymbol{\varphi}_r)$ can be denoted as

$$h_i(\boldsymbol{\varphi}_t, \varphi_r^i) = \log_2 \left(N_0 B + \sum_{k=1}^{N} p_t L^{k,i} G_t^{k,i}(\varphi_t^k) G_r^{k,i}(\varphi_r^i) \right), \tag{22}$$

$$g_i(\boldsymbol{\varphi}_t, \varphi_r^i) = \log_2 \left(N_0 B + \sum_{\substack{k=1 \\ k \neq i}}^{N} p_t L^{k,i} G_t^{k,i}(\varphi_t^k) G_r^{k,i}(\varphi_r^i) \right). \tag{23}$$

Note that there is a sum of multiple $G_t^{k,i}(\varphi_t^k) G_r^{k,i}(\varphi_r^i)$ terms in both logarithmic functions $h_i(\boldsymbol{\varphi}_t, \varphi_r^i)$ and $g_i(\boldsymbol{\varphi}_t, \varphi_r^i)$, we first discuss the values of $G_t^{k,i}(\varphi_t^k) G_r^{k,i}(\varphi_r^i)$ terms.

To discuss the values of $G_t^{k,i}(\varphi_t^k) G_r^{k,i}(\varphi_r^i)$ terms, we observe the piecewise property of $G_t(\varphi_t)$ and $G_r(\varphi_r)$, which is quite challenging to handle. Therefore, we try to determine the ranges of φ_t and φ_r, so that the piecewise property of $G_t(\varphi_t)$ and $G_r(\varphi_r)$ can be taken off. Then, as suggested at the beginning of this subsection, the real positions of Txs and Rxs are assumed to be certain, which implies the alignment angle error matrix $\boldsymbol{\theta}_\gamma (\gamma \in \{t, r\})$ between Txs and Rxs is determined. Thus, with the determined alignment angle error matrix $\boldsymbol{\theta}_\gamma (\gamma \in \{t, r\})$, the piecewise property of $G_t(\varphi_t)$ and $G_r(\varphi_r)$ can be removed by choosing appropriate ranges of beamwidths $\boldsymbol{\varphi}_t$ and $\boldsymbol{\varphi}_r$ via the following procedures:

1) In order to ensure the target Tx/Rx is covered by the main beam, φ_γ^i should satisfy $\varphi_\gamma^i \geq 2|\theta_\gamma^{i,i}|$, where $\gamma \in \{t, r\}$. Then, the antenna gain for the i^{th} link between Tx i and Rx i is given as

$$G_\gamma^{i,i}(\varphi_\gamma^i) = \frac{2\pi - (2\pi - \varphi_\gamma^i) g}{\varphi_\gamma^i}, \ \gamma \in \{t, r\}, \forall i. \tag{24}$$

2) In order not to cover other Txs/Rxs as far as possible, φ_t^i should satisfy $\varphi_t^i \leq 2|\theta_t^{i,l}|$, where $|\theta_t^{i,l}| = \min(|\theta_t^{i,j}|)$, $|\theta_t^{i,j}| > |\theta_t^{i,i}|$, $j \in \{1, \cdots, N\}$, $j \neq i$; likewise, we have $\varphi_r^i \leq 2|\theta_r^{l,i}|$, where $|\theta_r^{l,i}| = \min(|\theta_r^{j,i}|)$, $|\theta_r^{j,i}| > |\theta_r^{i,i}|$, $j \in \{1, \cdots, N\}$, $j \neq i$. Thus, the antenna gains ${G_t}^{i,j}(\varphi_t^i)$ and ${G_r}^{j,i}(\varphi_r^i)$ for the link between Tx i and Rx j can be determined and calculated as (25), which takes off the piecewise property of antenna gains and makes the antenna gains become convex functions for specific links.

$${G_t}^{i,j}(\varphi_t^i) = \begin{cases} \dfrac{2\pi - (2\pi - \varphi_t^i) g}{\varphi_t^i}, & |\theta_t^{i,j}| \leq |\theta_t^{i,i}|, \\ g, & |\theta_t^{i,j}| > |\theta_t^{i,i}|, \end{cases} \tag{25a}$$

$${G_r}^{j,i}(\varphi_r^i) = \begin{cases} \dfrac{2\pi - (2\pi - \varphi_r^i) g}{\varphi_r^i}, & |\theta_r^{j,i}| \leq |\theta_r^{i,i}|, \\ g, & |\theta_r^{j,i}| > |\theta_r^{i,i}|. \end{cases} \quad (j \in \{1, \cdots, N\} \quad \text{and} \quad j \neq i) \tag{25b}$$

Hence, for the functions $h_i(\boldsymbol{\varphi}_t, \varphi_r^i)$ in (22) and $g_i(\boldsymbol{\varphi}_t, \varphi_r^i)$ in (23), there are four cases for $G_t^{k,i}(\varphi_t^k) G_r^{k,i}(\varphi_r^i)$:

1) When $|\theta_t^{k,i}| > |\theta_t^{k,k}|$ and $|\theta_r^{k,i}| > |\theta_r^{i,i}|$,

$$G_t^{k,i}(\varphi_t^k) G_r^{k,i}(\varphi_r^i) = g^2. \tag{26}$$

2) When $|\theta_t^{k,i}| \leq |\theta_t^{k,k}|$ and $|\theta_r^{k,i}| > |\theta_r^{i,i}|$,

$$G_t^{k,i}(\varphi_t^k) G_r^{k,i}(\varphi_r^i) = g \cdot \frac{2\pi - (2\pi - \varphi_t^k) g}{\varphi_t^k}. \tag{27}$$

3) When $|\theta_t^{k,i}| > |\theta_t^{k,k}|$ and $|\theta_r^{k,i}| \leq |\theta_r^{i,i}|$,

$$G_t^{k,i}(\varphi_t^k) G_r^{k,i}(\varphi_r^i) = g \cdot \frac{2\pi - (2\pi - \varphi_r^i) g}{\varphi_r^i}. \tag{28}$$

4) When $|\theta_t^{k,i}| \leq |\theta_t^{k,k}|$ and $|\theta_r^{k,i}| \leq |\theta_r^{i,i}|$,

$$G_t^{k,i}(\varphi_t^k) G_r^{k,i}(\varphi_r^i) = \frac{2\pi - (2\pi - \varphi_t^k) g}{\varphi_t^k} \cdot \frac{2\pi - (2\pi - \varphi_r^i) g}{\varphi_r^i}. \tag{29}$$

According to the above analysis of the possible cases for $G_t^{k,i}(\varphi_t^k) G_r^{k,i}(\varphi_r^i)$, it can be inferred that, with the determined alignment angle error matrix $\boldsymbol{\theta}_\gamma (\gamma \in \{t, r\})$ and appropriately selected ranges for beamwidths $\boldsymbol{\varphi}_t$ and $\boldsymbol{\varphi}_r$, $h_i(\boldsymbol{\varphi}_t, \varphi_r^i)$ in (22) and $g_i(\boldsymbol{\varphi}_t, \varphi_r^i)$ in (23) can both be denoted as the form

$$log_2 \left(\sum_{i=1}^{n} \frac{a_i}{x_i y_i} + \sum_{i=1}^{m} \frac{b_i}{z_i} + c \right), \tag{30}$$

where a_i, b_i, and c are all positive consts, x_i, y_i, and z_i are positive variables, representing φ_t and φ_r.

Lemma 1: The function $f(\boldsymbol{x}, \boldsymbol{y}, \boldsymbol{z})$ is a convex function when variables $\boldsymbol{x}$, $\boldsymbol{y}$, $\boldsymbol{z}$ and parameters $\boldsymbol{a}$, $\boldsymbol{b}$, c are all positive.

$$f(\boldsymbol{x}, \boldsymbol{y}, \boldsymbol{z}) = log_2 \left(\sum_{i=1}^{n} \frac{a_i}{x_i y_i} + \sum_{i=1}^{m} \frac{b_i}{z_i} + c \right) \tag{31}$$

Proof: See Appendix A.

Hence, the functions $h_i(\boldsymbol{\varphi}_t, \varphi_r^i)$ in (22) and $g_i(\boldsymbol{\varphi}_t, \varphi_r^i)$ in (23) are both convex functions. Moreover, the functions $h(\boldsymbol{\varphi}_t, \boldsymbol{\varphi}_r)$ in (20) and $g(\boldsymbol{\varphi}_t, \boldsymbol{\varphi}_r)$ in (21) are also convex functions.

Thus, the problem in (19) can be rewritten as

$$\min_{\boldsymbol{\varphi}_t, \boldsymbol{\varphi}_r} \ g(\boldsymbol{\varphi}_t, \boldsymbol{\varphi}_r) - h(\boldsymbol{\varphi}_t, \boldsymbol{\varphi}_r) \tag{32a}$$

$$\text{s.t. } \varphi_t^i \geq 2|\theta_t^{i,i}|, \quad \forall i \tag{32b}$$

$$\varphi_r^i \geq 2|\theta_r^{i,i}|, \quad \forall i \tag{32c}$$

$$\varphi_t^i \leq 2|\theta_t^{i,l}|, \quad \forall i$$
$$(|\theta_t^{i,l}| = \min(|\theta_t^{i,j}|), |\theta_t^{i,j}| > |\theta_t^{i,i}|,$$
$$j \in \{1, \cdots, N\}, \ j \neq i) \tag{32d}$$

$$\varphi_r^i \leq 2|\theta_r^{l,i}|, \quad \forall i$$

$$|\theta_r^{l,i}| = \min(|\theta_r^{j,i}|), (|\theta_r^{j,i}| > |\theta_r^{i,i}|, \quad j \in \{1, \cdots, N\},\ j \neq i) \tag{32e}$$
(9b), (9c).

Since the functions $g(\boldsymbol{\varphi}_t, \boldsymbol{\varphi}_r)$ in (21) and $h(\boldsymbol{\varphi}_t, \boldsymbol{\varphi}_r)$ in (20) are both convex functions, the optimization object in problem (32) is regarded as a difference of two convex functions, making the problem (32) a standard D.C. problem.

Thus, we can solve a sequence of convex approximations of problem (32) iteratively to obtain the solutions. By linearizing the convex function $h(\boldsymbol{\varphi}_t, \boldsymbol{\varphi}_r)$, the convex approximation of problem (32) at κ-th iteration is given as

$$\min_{\boldsymbol{\varphi}_t, \boldsymbol{\varphi}_r}\ g(\boldsymbol{\varphi}_t, \boldsymbol{\varphi}_r) - h(\boldsymbol{\varphi}_t{}^{(\kappa)}, \boldsymbol{\varphi}_r{}^{(\kappa)}) - \langle \nabla(h_t(\boldsymbol{\varphi}_t{}^{(\kappa)}), h_r(\boldsymbol{\varphi}_r{}^{(\kappa)})), (\boldsymbol{\varphi}_t, \boldsymbol{\varphi}_r) - (\boldsymbol{\varphi}_t{}^{(\kappa)}, \boldsymbol{\varphi}_r{}^{(\kappa)}) \rangle$$
$$\text{s.t. (32b), (32c), (32d), (32e), (9b), (9c).} \tag{33a}$$

The function $h(\boldsymbol{\varphi}_t, \boldsymbol{\varphi}_r)$'s gradient is given as

$$\nabla h(\boldsymbol{\varphi}_t, \boldsymbol{\varphi}_r) = \left[\frac{\partial h}{\partial \varphi_t^1}, \cdots, \frac{\partial h}{\partial \varphi_t^N}, \frac{\partial h}{\partial \varphi_r^1}, \cdots, \frac{\partial h}{\partial \varphi_r^N} \right]^T, \tag{34}$$

where

$$\frac{\partial h}{\partial \varphi_t^k} = \frac{B}{ln2} \cdot \sum_{i=1}^{N} \frac{p_t L^{k,i} G_t'^{k,i}(\varphi_t^k) G_r^{k,i}(\varphi_r^i)}{N_0 B + \sum_{k=1}^{N} p_t L^{k,i} G_t^{k,i}(\varphi_t^k) G_r^{k,i}(\varphi_r^i)}, \tag{35}$$

$$\frac{\partial h}{\partial \varphi_r^i} = \frac{B}{ln2} \cdot \frac{\sum_{k=1}^{N} p_t L^{k,i} G_t^{k,i}(\varphi_t^k) G_r'^{k,i}(\varphi_r^i)}{N_0 B + \sum_{k=1}^{N} p_t L^{k,i} G_t^{k,i}(\varphi_t^k) G_r^{k,i}(\varphi_r^i)}, \tag{36}$$

and $k, i \in \{1, \cdots, N\}$.

In (35) and (36), the $G_t'^{k,i}(\varphi_t^k)$ and $G_r'^{k,i}(\varphi_r^i)$ are given as

$$G_t'^{k,i}(\varphi_t^k) = \begin{cases} -\frac{2\pi(1-g)}{{\varphi_t^k}^2}, & \text{if } |\theta_t^{k,i}| \leq |\theta_t^{k,k}|, \\ 0, & \text{if } |\theta_t^{k,i}| > |\theta_t^{k,k}|, \end{cases} \tag{37}$$

$$G_r'^{k,i}(\varphi_r^i) = \begin{cases} -\frac{2\pi(1-g)}{{\varphi_r^i}^2}, & \text{if } |\theta_r^{k,i}| \leq |\theta_r^{i,i}|, \\ 0, & \text{if } |\theta_r^{k,i}| > |\theta_r^{i,i}|. \end{cases} \tag{38}$$

Thus, the problem (33) can be efficiently solved by available convex software packages [39].

Furthermore, since $h(\boldsymbol{\varphi}_t, \boldsymbol{\varphi}_r)$ is a convex function, we have

$$h(\boldsymbol{\varphi}_t, \boldsymbol{\varphi}_r) \geq h(\boldsymbol{\varphi}_t^{(\kappa)}, \boldsymbol{\varphi}_r^{(\kappa)}) + \langle \nabla(h_t(\boldsymbol{\varphi}_t{}^{(\kappa)}), h_r(\boldsymbol{\varphi}_r{}^{(\kappa)})), (\boldsymbol{\varphi}_t, \boldsymbol{\varphi}_r) - (\boldsymbol{\varphi}_t{}^{(\kappa)}, \boldsymbol{\varphi}_r{}^{(\kappa)}) \rangle. \tag{39}$$

This feature provides a well approximated upper bound of minimization problem (32). As $(\boldsymbol{\varphi}_t^{(\kappa)}, \boldsymbol{\varphi}_r^{(\kappa)})$ is feasible to problem (33), it can be obtained that

$$g(\boldsymbol{\varphi}_t^{(\kappa+1)}, \boldsymbol{\varphi}_r^{(\kappa+1)}) - h(\boldsymbol{\varphi}_t^{(\kappa+1)}, \boldsymbol{\varphi}_r^{(\kappa+1)}) \leq g(\boldsymbol{\varphi}_t^{(\kappa)}, \boldsymbol{\varphi}_r^{(\kappa)}) - [h(\boldsymbol{\varphi}_t^{(\kappa)}, \boldsymbol{\varphi}_r^{(\kappa)}) + \langle \nabla(h_t(\boldsymbol{\varphi}_t{}^{(\kappa)}), h_r(\boldsymbol{\varphi}_r{}^{(\kappa)})), (\boldsymbol{\varphi}_t^{(\kappa+1)}, \boldsymbol{\varphi}_r^{(\kappa+1)}) - (\boldsymbol{\varphi}_t{}^{(\kappa)}, \boldsymbol{\varphi}_r{}^{(\kappa)}) \rangle]$$
$$\leq g(\boldsymbol{\varphi}_t^{(\kappa)}, \boldsymbol{\varphi}_r^{(\kappa)}) - h(\boldsymbol{\varphi}_t^{(\kappa)}, \boldsymbol{\varphi}_r^{(\kappa)}). \tag{40}$$

Since the constraint set is compact, the sequence $(\boldsymbol{\varphi}_t^{(\kappa)}, \boldsymbol{\varphi}_r^{(\kappa)})$ always converges.

Algorithm 1 The Overall Beamwidth Optimization Algorithm for Problem (16)

Input: Transmitted power p_t, noise density N_0, bandwidth B, sector widths $\boldsymbol{\psi}_t$, $\boldsymbol{\psi}_r$, estimated vehicular positions $(\hat{\boldsymbol{x}}, \hat{\boldsymbol{y}})$, alignment angle error matrix $\boldsymbol{\theta}_\gamma (\gamma \in \{t, r\})$

Output: The optimized beamwidths $\boldsymbol{\varphi}_t, \boldsymbol{\varphi}_r$

1: Initialize $\boldsymbol{\varphi}_t$ and $\boldsymbol{\varphi}_r$ with feasible values and set $\kappa = 0$;
2: **while** Not convergence **do**
3: Solve the problem (33) to obtain the solution $(\boldsymbol{\varphi}_t^*, \boldsymbol{\varphi}_r^*)$;
4: Set $\kappa = \kappa + 1$, $(\boldsymbol{\varphi}_t^{(\kappa)}, \boldsymbol{\varphi}_r^{(\kappa)}) = (\boldsymbol{\varphi}_t^*, \boldsymbol{\varphi}_r^*)$;
5: **end while**

The overall algorithm of problem (16) is summarized in Algorithm 1. Additionally, it should be noted that the computation complexity of solving problem (33) is $\mathcal{O}(N^3)$. Since this paper studies V2V communication between neighbor vehicles on the highway, the system size N is very small, the computation complexity of this algorithm is acceptable [40].

2) FINDING THE OPTIMAL BEAMWIDTHS BASED ON MONTE CARLO TESTS

The above subsection solves the problem (16), where the intractable probability density function $f(\boldsymbol{x}, \boldsymbol{y})$ is set aside from problem (10), indicating the real positions of Txs and Rxs are certain. Therefore, in this subsection, considering the uncertainty of vehicular real positions, Monte Carlo method is utilized to simulate $f(\boldsymbol{x}, \boldsymbol{y})$ by generating S different sets of the assumed certain real positions for Txs and Rxs in the system. Then, with the beamwidths optimized by the above proposed Algorithm 1 for S different Monte Carlo sets, a potential range for the final optimal beamwidths can be obtained. Furthermore, denote the ι^{th} potential optimal beamwidths as $\boldsymbol{\varphi}_{t,\iota}$ and $\boldsymbol{\varphi}_{r,\iota}$, substitute $\boldsymbol{\varphi}_{t,\iota}$ and $\boldsymbol{\varphi}_{r,\iota}$ into formula (41), as shown at the bottom of the page, to obtain the average transmission throughput $R(\boldsymbol{\varphi}_{t,\iota}, \boldsymbol{\varphi}_{r,\iota})$. The potential optimal beamwidths with the maximal average throughput are the optimal beamwidths $\boldsymbol{\varphi}_t{}^*$ and $\boldsymbol{\varphi}_r{}^*$. Additionally, it should be noted that, since the probability density function $f(\boldsymbol{x}, \boldsymbol{y})$ is simulated by Monte Carlo tests, the probability density function in the proposed Gaussian-distributed position error model can be substituted by any realistic position error distribution in practice, which is of much adaptability.

$$R(\boldsymbol{\varphi}_{t,\iota}, \boldsymbol{\varphi}_{r,\iota}) = \left\{ \sum_{s=1}^{S} \left[\sum_{i=1}^{N} B \cdot \log_2 \left(1 + \frac{p_t L_s^{i,i} G_t(\theta_{t,s}^{i,i}, \varphi_{t,\iota}^i) G_r(\theta_{r,s}^{i,i}, \varphi_{r,\iota}^i)}{N_0 B + \sum_{k \neq i}^{N} p_t L^{k,i} G_t(\theta_{t,s}^{k,i}, \varphi_{t,\iota}^k) G_r(\theta_{r,s}^{k,i}, \varphi_{r,\iota}^i)} \right) \right] \right\} \Big/ S, \tag{41}$$

Algorithm 2 A Basic Monte Carlo (B-MC) Based Optimal Beamwidths Finding Algorithm

Input: The estimated vehicular position coordinates $(\hat{\boldsymbol{x}}, \hat{\boldsymbol{y}})$, the position error variances $\boldsymbol{\sigma}_X^2$, $\boldsymbol{\sigma}_Y^2$, vehicular link number N, Monte Carlo Gaussian sampling size S

Output: The optimal beamwidths $\boldsymbol{\varphi}_t{}^*$, $\boldsymbol{\varphi}_r{}^*$

1: Generate S sets of the Txs and Rxs' assumed certain real position coordinates $(\boldsymbol{x}, \boldsymbol{y})$, which should follow the corresponding Gaussian-distributed position error model;
2: Calculate the optimized beamwidth matrixes Φ_t and Φ_r for the S sets of the N pairs of Txs and Rxs in the system by Algorithm 1. Matrixes Φ_t and Φ_r are of N lines and S columns;
3: **for** The beamwidths $\boldsymbol{\varphi}_{t,\iota}$ and $\boldsymbol{\varphi}_{r,\iota}$ in the ι^{th} column of Φ_t and Φ_r **do**
4: With all S sets of alignment angle error matrix $\boldsymbol{\theta}_{\gamma,s}$ $(\gamma \in \{t, r\})$, calculate the average transmission throughput $R(\boldsymbol{\varphi}_{t,\iota}, \boldsymbol{\varphi}_{r,\iota})$ via formula (41);
5: **end for**
6: The optimal beamwidths $(\boldsymbol{\varphi}_t{}^*, \boldsymbol{\varphi}_r{}^*) = \arg\max R(\boldsymbol{\varphi}_{t,\iota}, \boldsymbol{\varphi}_{r,\iota}), \iota \in \{1, \cdots, S\}$.

Algorithm 3 A Modified Monte Carlo (M-MC) Based Optimal Beamwidths Finding Algorithm

Input: The estimated vehicular position coordinates $(\hat{\boldsymbol{x}}, \hat{\boldsymbol{y}})$, the position error variances $\boldsymbol{\sigma}_X^2$,$\boldsymbol{\sigma}_Y^2$, vehicular link number N, Monte Carlo Gaussian sampling size S, uniform sampling size U

Output: The optimal beamwidths $\boldsymbol{\varphi}_t{}^*$, $\boldsymbol{\varphi}_r{}^*$

1: Same as the **Step 1** and **Step 2** in Algorithm 2;
2: Get the maximal optimized beamwidth sequences $\boldsymbol{\phi}_t$ and $\boldsymbol{\phi}_r$, whose elements satisfy $\phi_{t,i} = \max(\Phi_t^{i,1}, \cdots, \Phi_t^{i,S})$, $\phi_{r,i} = \max(\Phi_r^{i,1}, \cdots, \Phi_r^{i,S})$, $i \in \{1, \cdots, N\}$;
3: In the scope of $[\boldsymbol{\phi}_t/2, \boldsymbol{\phi}_t]$ and $[\boldsymbol{\phi}_r/2, \boldsymbol{\phi}_r]$, uniformly and randomly generate U sets of beamwidths $\{\boldsymbol{\varphi}_{t,1}, \cdots, \boldsymbol{\varphi}_{t,U}\}$ and $\{\boldsymbol{\varphi}_{r,1}, \cdots, \boldsymbol{\varphi}_{r,U}\}$ for the N pairs of the Txs and Rxs;
4: **for** The ι^{th} set of beamwidths $\boldsymbol{\varphi}_{t,\iota}$ and $\boldsymbol{\varphi}_{r,\iota}$ in the above generated U sets **do**
5: With all S sets of alignment angle error matrix $\boldsymbol{\theta}_{\gamma,s}$ $(\gamma \in \{t, r\})$, calculate the average transmission throughput $R(\boldsymbol{\varphi}_{t,\iota}, \boldsymbol{\varphi}_{r,\iota})$ via formula (41);
6: **end for**
7: The optimal beamwidths $(\boldsymbol{\varphi}_t{}^*, \boldsymbol{\varphi}_r{}^*) = \arg\max R(\boldsymbol{\varphi}_{t,\iota}, \boldsymbol{\varphi}_{r,\iota}), \iota \in \{1, \cdots, U\}$.

Then, based on the above idea, the Basic Monte Carlo (B-MC) based optimal beamwidths finding algorithm is proposed in Algorithm 2.

However, since the potential optimal beamwidths scope is raw from the Monte Carlo tests in Algorithm 2, the optimal beamwidths finding procedures in B-MC are quite inefficient. Hence, to improve the optimal beamwidths finding efficiency, the Modified Monte Carlo (M-MC) based optimal beamwidths finding algorithm is proposed in Algorithm 3. In Algorithm 3, S sets of the optimized beamwidths are first calculated same as **Step 1-2** in Algorithm 2. Then, the maximal optimized beamwidth sequences ϕ_t and ϕ_r are obtained. Considering the distribution of optimized beamwidths, which will be demonstrated in Section IV, the final optimal beamwidths lay in the range of $[\boldsymbol{\phi}_t/2, \boldsymbol{\phi}_t]$ and $[\boldsymbol{\phi}_r/2, \boldsymbol{\phi}_r]$. Thus, U sets of the potential optimal beamwidths candidates are uniformly and randomly generated within this range. Next, substitute the candidate beamwidths into (41) to calculate the average transmission throughput, the one with the maximal average transmission throughput corresponds to the optimal beamwidths.

The proposed MCBO method, especially with M-MC algorithm, can lessen the high computation complexity caused by fine discretization zone precision in the discretization-based beamwidth optimization method. Nevertheless, with the increment of system size, the potential optimal beamwidth candidate space in MCBO method will still experience a quick growth, which also results in high computation complexity. Therefore, a simple and approximated grouping strategy is proposed in MCBO method to reduce the optimization scale in the system.

The grouping criterion is illustrated in Fig. 3, where the estimated vehicular positions are represented by red dots. The

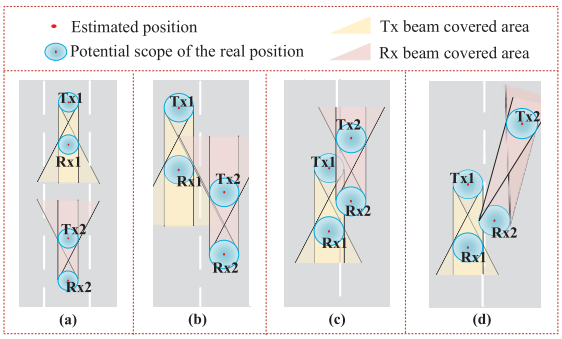

FIGURE 3. The grouping criterion.

blue ellipse denotes the potential scope of the real vehicular position. The yellow area is the overestimated Tx beam covered area, and the reddish area is the overestimated Rx beam covered area. These overestimated beam covered areas can be obtained by geometry approaches. The following are the detailed explanations of the grouping criterion.

- As shown in Fig. 3 (a), four vehicles run in the same lane one after the other. The inter-vehicle distances between Tx1&Rx1, Rx1&Tx2, and Tx2&Rx2 should be kept as several tens of meters. Considering the accumulated long distance between Tx1&Rx2, the interference from Tx1 to Rx2 can be neglected. Thus, the two links can be separated into two groups.
- As shown in Fig. 3 (b), if the shortest distance between the potential scope of Tx1's real position and the potential scope of Rx2's real position is larger than a certain distance, Rx2 is considered to receive little interference from Tx1. Hence, the two links can be separated into two

TABLE 1. Simulation parameters.

Parameter	Value	
Sector width ($\psi_{t/r}$)	30°	
Transmit power (p_t)	23 dBm	[33]
Receiver noise figure (n_r)	13 dB	[33]
Noise power spectral density (N_0)	-174 dBm/Hz	
Bandwidth (B)	200 MHz	[33]
Carrier frequency (f)	30 GHz	[33]
Antenna gain of the side beam (g)	0.05	[16]

groups. Otherwise, there is a chance that Tx1 may cause interference to Rx2 and whether the two links should stay in one group needs further judgements as below.

- As shown in Fig. 3 (c), the potential scope of Rx2's real position is in the overestimated beam covered area of Tx1. Meanwhile, the potential scope of Tx1's real position is also in the overestimated beam covered area of Rx2, which implies the potential reception direction of Rx2. Thus, there is a chance that Tx1 may cause severe interference to Rx2. Hence, these two links should stay in one group for beamwidth optimization.
- As shown in Fig. 3 (d), the potential scope of Rx2's real position is still in the overestimated beam covered area of Tx1. However, the potential scope of Tx1's real position is not in the overestimated beam covered area of Rx2. Thus, Rx2 will receive little interference from Tx1. Hence, these two links can be separated into two groups.

As aforementioned, since the severe interference only come from the vehicular links running on the neighbor lanes in a small distance range, with the above grouping strategy, the system scale can be limited to a very small size, which can be considered as the lane number at most. Thus, the potential optimal beamwidth candidate space in the MCBO method is of small scale. Moreover, the **step 3-5** in B-MC algorithm and **step 4-6** in M-MC algorithm can be calculated using parallel computing. A new system-on-a-chip (SoC) called Orin developed by NVIDIA is able to provide 200 trillion operations per second (TOPS) for autonomous machines [41], which is adequate for the calculation of our proposed MCBO method in highway V2V communication.

IV. SIMULATION RESULTS

In this section, simulation results are presented to validate the effectiveness of the proposed overhead-free beam alignment scheme and beamwidth optimization method over the single-link scenario and multi-link scenario. In the simulation, the evaluation parameters including bandwidth, carrier frequency, transmit power, and receiver noise figure, are configured in accordance to 3GPP TR 37.885 [33]. Unless stated otherwise, simulation parameters summarized in Table 1 are utilized in both single-link and multi-link scenarios.

A. SINGLE-LINK SCENARIO

1) A SIMPLE CASE

For the single-link scenario, this subsection first focuses on a simple case, where the communication distance is set as 80 m

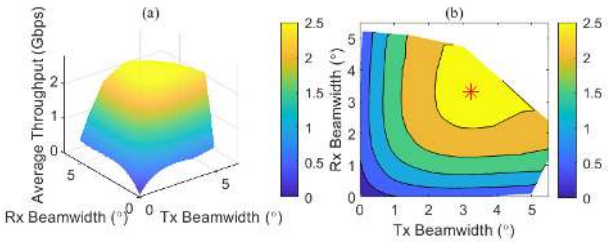

FIGURE 4. (a) The spatial average throughput surface fitted by the 2000 sets of data. (b) The contour map of the average throughput fitted by the 2000 sets of data.

and the position error standard deviations are set as $\sigma_X = 1$ m, $\sigma_Y = 1$ m for both Tx and Rx.

To explore the average throughput performance in the raw potential optimal beamwidths searching scope and present the result visually, the B-MC algorithm in MCBO method is first applied in the simple case for beamwidth optimization with Monte Carlo Gaussian sampling size $S = 2000$.

Therefore, in **Step 3-5** in Algorithm 2, with the optimized beamwidths of Txs and Rxs, 2000 sets of the average throughputs are calculated. Then, a spatial average throughput surface is obtained in Fig. 4 (a) by fitting the above 2000 sets of data. Fig. 4 (b) shows the correlated contour map. According to **Step 6** in Algorithm 2, the optimal beamwidths are $\varphi_t^* = 3.3°$ and $\varphi_r^* = 3.2°$, which correspond to the highest point 2.64 Gbps in Fig. 4 (a) and the red point in Fig. 4 (b).

To show the comparison between the B-MC algorithm and M-MC algorithm, Fig. 5 exhibits their convergence speeds in the final optimal beamwidths and maximal average throughput finding procedures, which indicates the Monte Carlo Gaussian sampling size S in B-MC algorithm and the uniform sampling size U in M-MC algorithm. Apparently, compared to B-MC algorithm, M-MC algorithm has a faster convergence speed finding the optimal beamwidths and maximal average throughput, which can lessen much computation complexity and is more suitable for practice.

2) A SINGLE-LINK WITH DIFFERENT POSITION ERRORS

Fig. 6 illustrates the influences of position error on the optimal beamwidths and the maximal average throughput when communication distance is set as 80 m. For visual presentation, the optimal beamwidths and the maximal average throughput are calculated by B-MC algorithm with Gaussian sampling size $S = 2000$. As shown in Fig. 6, with the increment of the position error, the optimal beamwidths of Tx and Rx will increase while the maximal average throughput will decrease. This is easy to understand, when the position error increases, the potential scope of Tx/Rx's real position becomes larger, and the covering beam becomes wider accordingly, resulting in smaller average throughput.

3) A SINGLE-LINK WITH DIFFERENT COMMUNICATION DISTANCES

Fig. 7 shows the impacts of communication distance on the optimal beamwidths and the maximal average throughput with the position error standard deviations $\sigma_X = 1$ m and

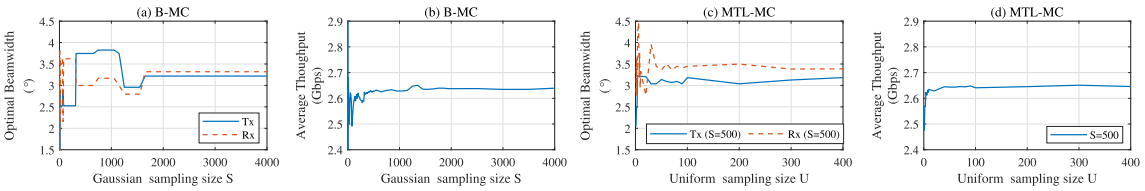

FIGURE 5. The convergence speed comparison between B-MC algorithm and M-MC algorithm when finding the optimal beamwidths and maximal average throughput.

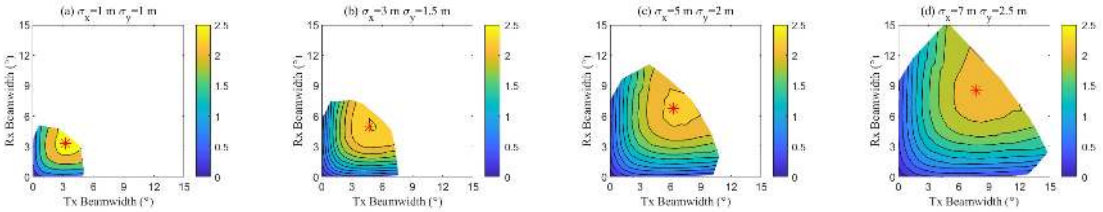

FIGURE 6. The influences of position error on the optimal beamwidths and the maximal average throughput.

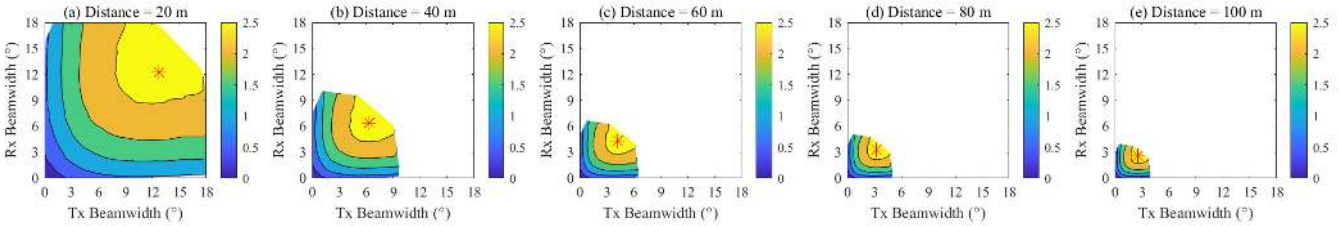

FIGURE 7. The impacts of communication distance on the optimal beamwidths and the maximal average throughput.

$\sigma_Y = 1$ m. For visual presentation, the optimal beamwidths of Tx/Rx and the maximal average throughput are also calculated by B-MC algorithm with Gaussian sampling size $S = 2000$. From Fig. 7, it can be inferred that when the communication distance grows, the optimal beamwidths for Tx and Rx will be narrowed down. This conforms to our intuitive expectation, because with the growth of the communication distance, the angle covering the same potential area will become thinner. In the meanwhile, with the given position error, in the simulated communication distance range (20 m to 100 m), communication distance has little effect on the maximal average throughput. This result indicates that with the growing communication distance, the increased antenna gain caused by narrower beam can compensate the increased pathloss caused by longer communication distance.

4) THE COMPARISONS BETWEEN THE PROPOSED SCHEME AND THE EXISTING INTERFERENCE UNDERESTIMATION SCHEME

Fig. 8 compares our proposed scheme and the existing interference underestimation scheme proposed in [16] over the throughput performances in the single-link scenario.

The existing interference underestimation scheme proposed in [16] is a typical example of the widely-adopted beam-sweeping-based beam alignment schemes. In this scheme, the fundamental beamwidth optimization tradeoff is between antenna gain and transmission time. It is because even though narrow beamwidth can bring high antenna gain, it also lengthens the beam alignment overhead in the transmission slot, which implies to shorten transmission time. This beamwidth optimization problem can be solved by the interference underestimation method proposed in [16], which ignores the interferences in the optimization problem due to the directionality of narrow beams. Then, in the proposed single link scenario, according to the evaluation parameters from [16], suppose the pilot transmission time $T_p = 20\ \mu s$, the transmission slot T_s satisfies $T_p/T_s = 0.01$, the relationship between communication distance and the throughput of the interference underestimation scheme is exhibited in the blue line in Fig. 8.

In our proposed scheme, the M-MC algorithm in MCBO method is applied for beamwidth optimization with Monte Carlo Gaussian sampling size S=500 and uniform sampling size U=400. The average throughput performances with different position errors are demonstrated in the red lines in Fig. 8.

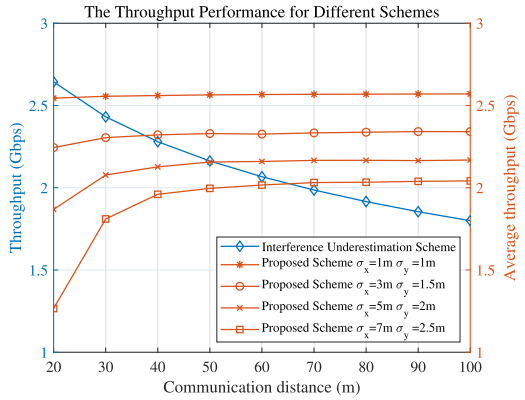

FIGURE 8. The comparisons of the throughput performances between the proposed scheme and the interference underestimation scheme proposed in [16].

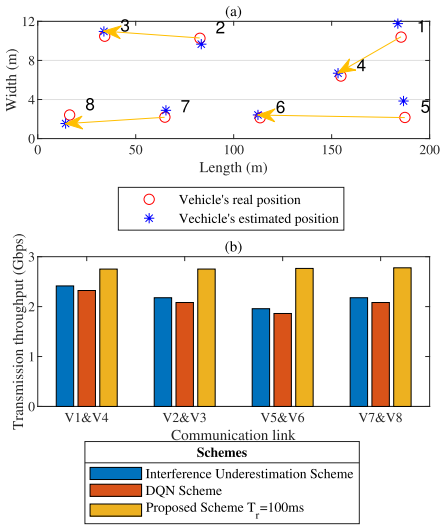

FIGURE 9. (a) The map of vehicular positions at the beginning of position refresh period. (b) The real throughput performance for each vehicular link with different schemes.

In Fig. 8, the communication distance is set from 20 m to 100 m. Despite the existing interference underestimation scheme can obtain the real throughput performance, and our proposed scheme can only obtain the average throughput performance of the Rx's nearby region, Fig. 8 still illustrates that when the communication distance is long, the proposed scheme has a better performance than the existing interference underestimation scheme. For instance, when the communication distance equals 100 m, compared to the existing interference underestimation scheme, the proposed scheme can provide 13.44% to 42.78% average throughput increments in the given four position error cases. Furthermore, consistent with the aforementioned conclusions, the proposed scheme with smaller position error or longer communication distance presents a larger performance gain compared to the existing interference underestimation scheme.

The above simulation results suggest that the proposed scheme has a better throughput performance when position error is small and communication distance is long, which is suitable for general car following cases on the highway. In such scene, for instance, when the vehicular speed is between 60 km/h to 120 km/h, suppose the car-following headway is 3 s, the inter-vehicle distance is about 50 m to 100 m, where our proposed scheme with small positioning errors outperforms the existing interference underestimation scheme. However, when communication distance is short, for instance, less than 20 m with the parameter configurations in this simulation, our proposed scheme is no longer suitable. Therefore, for these small distance cases, we can explore using a combination of our proposed scheme and the existing scheme for better beam alignment and beamwidth optimization.

B. MULTI-LINK SCENARIO

In the simulation setup of the multi-link scenario, the road configuration follows the descriptions for highway cases in 3GPP TR 37.885 [33]. As shown in Fig. 9 (a), we model a three-lane single direction highway road segment. Since we study the mmWave V2V communication between neighbor vehicles, the communication distance is quite limited compared to the road length specified in [33]. Thus, the road segment length is only set as 200 m in this simulation. Then, as described in 3GPP TR 36.885 [42], the vehicles of same size are dropped on the road segment according to spatial Poisson process and the vehicle density is determined by the vehicle speed, which is set as 70 km/h in this simulation. Furthermore, the V2V links are randomly formed between neighbor vehicles in the same lane or neighbor lanes. After the simulation setup, Fig. 9 (a) captures the vehicular positions at the beginning of position refresh period. Then, vehicles move forward, and in each V2V link, the front vehicle passes its sensor information to the rear vehicle via directional mmWave communication.

The simulation in this subsection aims to put our proposed scheme in a realistic scenario and compare our proposed scheme with the existing schemes, validating its effectiveness and feasibility in practice. Therefore, the position refresh period T_r is introduced in this simulation and is set as 100 ms, conforming to vehicle location update period specified in 3GPP TR 37.885 [33] and the BMS broadcasting period specified in SAE J2735 [43]. The position error standard deviations $\boldsymbol{\sigma}_X$ and $\boldsymbol{\sigma}_Y$ are set to be 1 m. Then, considering passenger comfort, the acceleration value is usually below 2 m/s^2 [44]. Referring to this acceleration range, the standard deviations of velocity error are set as $\sigma_{V_x} = 2$ m/s and $\sigma_{V_y} = 1$ m/s. Thus, according to formula (6), when $T_r = 100$ ms, the position error standard deviations of the mobile vehicle can still be approximated as 1 m. Additionally, with the estimated positions and position errors, the vehicular links in Fig. 9 (a) are grouped in accordance to the grouping criterion stated in Section III-B. As a result, all the vehicular links are separated into single-link cases.

TABLE 2. The Optimal Beamwidths for Each Vehicular Link of Different Schemes.

	V1&V4	V2&V3	V5&V6	V7&V8
Tx/Rx's optimal beamwidths of the interference underestimation scheme in [16] (°)	10.0	10.0	10.0	10.0
Tx/Rx's optimal beamwidths of the DQN scheme in [22] (°)	15.0	12.0	12.0	12.0
Tx/Rx's optimal beamwidths of the proposed scheme with $T_r = 100$ ms (°)	7.7/8.7	5.1/5.3	3.4/3.5	5.0/5.2

Next, the proposed scheme is compared with two baseline schemes, which are the interference underestimation scheme proposed in [16] and the deep Q network (DQN) scheme recently proposed in [22]. The interference underestimation scheme has been introduced previously and the DQN scheme still belongs to the widely-adopted beam-sweeping-based beam alignment category. The DQN scheme inherits the system throughput maximization problem from [16] but takes into account the interference in design and utilizes reinforcement learning to optimize beamwidths with low complexity. In this simulation, the DQN design is generally in consistence with that in [22]. The state contains the noise figure and the interfering channel gains from other Txs to this link's Rx, which are all normalized by this link's channel gain. The action is the combination of the beamwidths for Tx and Rx. The reward is set as the instantaneous effective sum rate. As aforementioned, the vehicular location is updated every 100 ms. Then, the state information is refreshed for each link at each location update. Moreover, a fully-connected neural network of three hidden layers with 300, 500, and 200 neurons is utilized. The initial learning rate is 0.001, batch size equals 32, and the network is updated by AdamOptimizer. ϵ-greedy policy is adopted during the training process. The initial ϵ value is set as 0.9. The learning rate will decrease and the ϵ value will increase gradually in the training process. The DQN experiments are run on a Linux server with the Intel Xeon CPU E5-2680 v4 of 2.40 GHz.

Table 2 demonstrates the optimal beamwidths for Tx/Rx of the interference underestimation scheme, the DQN scheme, and our proposed scheme with $T_r = 100$ ms. For our proposed scheme, M-MC algorithm with Gaussian sampling size $S = 500$ and uniform sampling size $U = 400$ is applied for beamwidth optimization in this simulation. Since MCBO is based on Monte Carlo method, the optimal beamwidths for Tx and Rx of the same link in Table 2 are not exactly the same. Accordingly, with the map in Fig. 9 (a) and the optimal beamwidths presented in Table 2, the real throughput performance for each vehicular link of our proposed scheme can be calculated by formula (8), where $\boldsymbol{\varphi}$ refers to the optimal beamwidth vector and $\boldsymbol{\theta}$ denotes the real alignment angle error matrix. The obtained real throughput performances for each vehicular link with different schemes are illustrated in Fig. 9 (b).

In Fig. 9 (b), the blue bars represent the interference underestimation scheme, the orange bars represent the DQN scheme, the yellow bars represent our proposed scheme with $T_r = 100$ ms. Because the interference underestimation scheme and the DQN scheme both belong to the beam-sweeping-based beam alignment category, which involves the beamwidth optimization tradeoff between antenna gain and transmission time, the optimal beamwidths optimized by these schemes are larger than those optimized by the proposed scheme in this simulation, resulting in lower antenna gains. Moreover, the beam alignment in these schemes costs alignment time, which reduces transmission time. Hence, lower antenna gain and less transmission time both lead to decreased throughput performances of these two schemes. As shown in Fig. 9 (b), our proposed scheme with $T_r = 100$ ms has 13.99% (V1&V4) to 41.23% (V5&V6) throughput gain than the interference underestimation scheme, and 18.48% (V1&V4) to 48.47% (V5&V6) throughput gain than the DQN scheme. Obviously, our proposed scheme with $T_r = 100$ ms achieves superior throughput performance than the baseline schemes in the proposed realistic highway V2V communication scenario, validating the effectiveness and feasibility of our proposed scheme in practice.

V. SUMMARY AND CONCLUSION

In this paper, we focus on the mmWave V2V communication between neighbor vehicles running in the same direction on the highway scenario and it is assumed that vehicles are able to obtain the position information of other vehicles. In such high mobility environment, the widely-adopted beam-sweeping-based beam alignment scheme will become inefficient due to Doppler spread.

To overcome the deficiency of the beam-sweeping-based beam alignment scheme and improve the throughput performance of mmWave V2V communication in highway scenario, we propose a vehicular-position-based overhead-free beam alignment scheme, in which the beam is directly steered to the estimated vehicular position without any searching steps in beam training. Then, a corresponding tailored beamwidth optimization problem is formulated to both avoid beam misalignment caused by localization errors and maximize transmission throughput. Afterwards, the MCBO method is developed to divide this optimization into two phases and solve this problem statistically.

Simulation results validate the capability of the proposed vehicular-position-based overhead-free beam alignment scheme and the MCBO method over single-link and multi-link scenarios. Comparing to the existing beam-sweeping-based beam alignment schemes, simulation results show that our proposed design can provide significant throughput improvements in general car-following scenarios on the highway.

Future research will be directed towards applying the proposed beam alignment scheme with beamwidth optimization method to urban scenarios. Considering the more

complicated channel and higher vehicle density, we will explore the combination of the proposed vehicular-position-based beam alignment scheme and the beam-sweeping-based beam alignment schemes to improve the system performance with small computation complexity in urban scenarios.

APPENDIX A
PROOF OF LEMMA 1

For the function $f(\boldsymbol{x},\boldsymbol{y},\boldsymbol{z}) = log_2(\sum_{i=1}^{n}\frac{a_i}{x_i y_i}+\sum_{i=1}^{m}\frac{b_i}{z_i}+c)$, variables $\boldsymbol{x},\boldsymbol{y},\boldsymbol{z}$ and parameters $\boldsymbol{a},\boldsymbol{b},c$ are all positive. We have

$$\begin{aligned}&\xi f(\boldsymbol{x}_1,\boldsymbol{y}_1,\boldsymbol{z}_1)+(1-\xi)f(\boldsymbol{x}_2,\boldsymbol{y}_2,\boldsymbol{z}_2)\\&= log_2\Bigg(\left(\sum_{i=1}^{n}\frac{a_i}{x_{1,i}y_{1,i}}+\sum_{i=1}^{m}\frac{b_i}{z_{1,i}}+c\right)^{\xi}\\&\quad\cdot\left(\sum_{i=1}^{n}\frac{a_i}{x_{2,i}y_{2,i}}+\sum_{i=1}^{m}\frac{b_i}{z_{2,i}}+c\right)^{(1-\xi)}\Bigg),\end{aligned}\tag{42}$$

where ξ is with $0\le\xi\le 1$. Then, by ignoring the cross terms, we have

$$\begin{aligned}&\left(\sum_{i=1}^{n}\frac{a_i}{x_{1,i}y_{1,i}}+\sum_{i=1}^{m}\frac{b_i}{z_{1,i}}+c\right)^{\xi}\\&\quad\cdot\left(\sum_{i=1}^{n}\frac{a_i}{x_{2,i}y_{2,i}}+\sum_{i=1}^{m}\frac{b_i}{z_{2,i}}+c\right)^{(1-\xi)}\qquad(43a)\\&\ge\left(\sum_{i=1}^{n}\frac{a_i}{x_{1,i}y_{1,i}}\right)^{\xi}\cdot\left(\sum_{i=1}^{n}\frac{a_i}{x_{2,i}y_{2,i}}\right)^{(1-\xi)}\\&\quad+\left(\sum_{i=1}^{m}\frac{b_i}{z_{1,i}}\right)^{\xi}\cdot\left(\sum_{i=1}^{m}\frac{b_i}{z_{2,i}}\right)^{(1-\xi)}+c\qquad(43b)\\&\ge\sum_{i=1}^{n}\left(\frac{a_i}{x_{1,i}y_{1,i}}\right)^{\xi}\left(\frac{a_i}{x_{2,i}y_{2,i}}\right)^{(1-\xi)}\\&\quad+\sum_{i=1}^{m}\left(\frac{b_i}{z_{1,i}}\right)^{\xi}\left(\frac{b_i}{z_{2,i}}\right)^{(1-\xi)}+c.\qquad(43c)\end{aligned}$$

Denote function $p(x,y)$ and $q(z)$ as

$$p(x,y) = log_2\left(\frac{a}{xy}\right),\tag{44}$$

$$q(z) = log_2\left(\frac{b}{z}\right),\tag{45}$$

where a and b are both positive consts. It is easy to prove that the function $p(x,y)$ and $q(z)$ are both convex functions. Therefore, according to the definition of convex function, we have

$$\begin{aligned}&\xi\cdot log_2\left(\frac{a}{x_1y_1}\right)+(1-\xi)\cdot log_2\left(\frac{a}{x_2y_2}\right)\\&\quad\ge log_2\left(\frac{a}{(\xi x_1+(1-\xi)x_2)(\xi y_1+(1-\xi)y_2)}\right),\qquad(46)\\&\xi\cdot log_2\left(\frac{b}{z_1}\right)+(1-\xi)\cdot log_2\left(\frac{b}{z_2}\right)\\&\quad\ge log_2\left(\frac{b}{(\xi z_1+(1-\xi)z_2)}\right).\qquad(47)\end{aligned}$$

Furthermore, we can obtain that

$$\left(\frac{a}{x_1y_1}\right)^{\xi}\left(\frac{a}{x_2y_2}\right)^{(1-\xi)}\ge\frac{a}{(\xi x_1+(1-\xi)x_2)(\xi y_1+(1-\xi)y_2)},\tag{48}$$

$$\left(\frac{b}{z_1}\right)^{\xi}\left(\frac{b}{z_2}\right)^{(1-\xi)}\ge\frac{b}{(\xi z_1+(1-\xi)z_2)}.\tag{49}$$

Therefore, we have

$$\begin{aligned}&log_2\Bigg(\sum_{i=1}^{n}\left(\frac{a_i}{x_{1,i}y_{1,i}}\right)^{\xi}\left(\frac{a_i}{x_{2,i}y_{2,i}}\right)^{(1-\xi)}\\&\quad+\sum_{i=1}^{m}\left(\frac{b_i}{z_{1,i}}\right)^{\xi}\left(\frac{b_i}{z_{2,i}}\right)^{(1-\xi)}+c\Bigg)\\&\ge log_2\Bigg(\sum_{i=1}^{n}\left(\frac{a_i}{(\xi x_{1,i}+(1-\xi)x_{2,i})(\xi y_{1,i}+(1-\xi)y_{2,i})}\right)\\&\quad+\sum_{i=1}^{m}\left(\frac{b_i}{\xi z_{1,i}+(1-\xi)z_{2,i}}\right)+c\Bigg).\end{aligned}\tag{50}$$

Thus, from formula (42)(43)(50), it can be proved that

$$\begin{aligned}&\xi f(\boldsymbol{x}_1,\boldsymbol{y}_1,\boldsymbol{z}_1)+(1-\xi)f(\boldsymbol{x}_2,\boldsymbol{y}_2,\boldsymbol{z}_2)\\&\ge log_2\Bigg(\sum_{i=1}^{n}\left(\frac{a_i}{(\xi x_{1,i}+(1-\xi)x_{2,i})(\xi y_{1,i}+(1-\xi)y_{2,i})}\right)\\&\quad+\sum_{i=1}^{m}\left(\frac{b_i}{\xi z_{1,i}+(1-\xi)z_{2,i}}\right)+c\Bigg)\\&= f\left(\xi\boldsymbol{x}_1+(1-\xi)\boldsymbol{x}_2,\xi\boldsymbol{y}_1+(1-\xi)\boldsymbol{y}_2,\xi\boldsymbol{z}_1+(1-\xi)\boldsymbol{z}_2\right).\end{aligned}\tag{51}$$

Hence, according to the definition of convex function, the function $f(\boldsymbol{x},\boldsymbol{y},\boldsymbol{z})$ is proved to be a convex function.

REFERENCES

[1] P. H. Rettore, G. Maia, L. A. Villas, and A. A. F. Loureiro, "Vehicular data space: The data point of view," *IEEE Commun. Surveys Tuts.*, vol. 21, no. 3, pp. 2392–2418, 3rd Quart., 2019.
[2] (Jul. 2015). *Samsung Safety Truck: Is It Actually All That Safe?* [Online]. Available: https://www.carkeys.co.uk/news/samsung-safety-truck-is-it-actually-all-that-safe
[3] M. Brambilla, M. Nicoli, G. Soatti, and F. Deflorio, "Augmenting vehicle localization by cooperative sensing of the driving environment: Insight on data association in urban traffic scenarios," *IEEE Trans. Intell. Transp. Syst.*, vol. 21, no. 4, pp. 1646–1663, Apr. 2020.
[4] *Enhancement of 3GPP Support for V2X Scenarios, Release 16*, document TS 22.186, 3GPP, Jun. 2019.
[5] *Study on Enhancement of 3GPP Support for 5G V2X Services (Release 16)*, document TR 22.886, 3GPP, Dec. 2018.
[6] J. B. Kenney, "Dedicated short-range communications (DSRC) standards in the united states," *Proc. IEEE*, vol. 99, no. 7, pp. 1162–1182, Jul. 2011.
[7] L. Zhao, X. Li, B. Gu, Z. Zhou, S. Mumtaz, V. Frascolla, H. Gacanin, M. I. Ashraf, J. Rodriguez, M. Yang, and S. Al-Rubaye, "Vehicular communications: Standardization and open issues," *IEEE Commun. Standards Mag.*, vol. 2, no. 4, pp. 74–80, Dec. 2018.
[8] K. Zrar Ghafoor, L. Kong, S. Zeadally, A. S. Sadiq, G. Epiphaniou, M. Hammoudeh, A. K. Bashir, and S. Mumtaz, "Millimeter-wave communication for Internet of Vehicles: Status, challenges, and perspectives," *IEEE Internet Things J.*, vol. 7, no. 9, pp. 8525–8546, Sep. 2020.

[9] A. N. Uwaechia and N. M. Mahyuddin, "A comprehensive survey on millimeter wave communications for fifth-generation wireless networks: Feasibility and challenges," *IEEE Access*, vol. 8, pp. 62367–62414, 2020.

[10] X. Wang, L. Kong, F. Kong, F. Qiu, M. Xia, S. Arnon, and G. Chen, "Millimeter wave communication: A comprehensive survey," *IEEE Commun. Surveys Tuts.*, vol. 20, no. 3, pp. 1616–1653, 3rd Quart., 2018.

[11] *Wireless LAN Medium Access Control (MAC) and Physical Layer (PHY) Specifications AMENDMENT 3: Enhancements for Very High Throughput in the 60 GHz Band (Adoption of IEEE Std 802.11ad-2012)*, IEEE Standard ISO/IEC/IEEE 802.11ad-2014, IEEE Computer Society, Mar. 2014.

[12] *IEEE Standard for Information Technology–Local and Metropolitan Area Networks–Specific Requirements—Part 15.3: Amendment 2: Millimeter-Wave-Based Alternative Physical Layer Extension*, IEEE Standard ISO/IEC/IEEE 802.15.3c-2009, IEEE Computer Society, Oct. 2009.

[13] P. Zhou, K. Cheng, X. Han, X. Fang, Y. Fang, R. He, Y. Long, and Y. Liu, "IEEE 802.11ay-based mmWave WLANs: Design challenges and solutions," *IEEE Commun. Surveys Tuts.*, vol. 20, no. 3, pp. 1654–1681, 3rd Quart., 2018.

[14] J. Mo, B. L. Ng, S. Chang, P. Huang, M. N. Kulkarni, A. Alammouri, J. C. Zhang, J. Lee, and W.-J. Choi, "Beam codebook design for 5G mmWave terminals," *IEEE Access*, vol. 7, pp. 98387–98404, 2019.

[15] T. Shimizu, V. Va, G. Bansal, and R. W. Heath, Jr., "Millimeter wave V2X communications: Use cases and design considerations of beam management," in *Proc. Asia–Pacific Microw. Conf. (APMC)*, Nov. 2018, pp. 183–185.

[16] H. Shokri-Ghadikolaei, L. Gkatzikis, and C. Fischione, "Beam-searching and transmission scheduling in millimeter wave communications," in *Proc. IEEE Int. Conf. Commun. (ICC)*, Jun. 2015, pp. 1292–1297.

[17] N. Eshraghi, V. Shah-Mansouri, and B. Maham, "Fair beamwidth selection and resource allocation for indoor millimeter-wave networks," in *Proc. IEEE Int. Conf. Commun. (ICC)*, May 2017, pp. 1–6.

[18] C. Pradhan, H. Chen, Y. Li, and B. Vucetic, "Joint beamwidth and energy optimization for multi-user millimeter wave communications," in *Proc. IEEE Int. Conf. Commun. Workshops (ICC Workshops)*, May 2018, pp. 1–6.

[19] A. Saeed and O. Gurbuz, "Joint power and beamwidth optimization for full duplex millimeter wave indoor wireless systems," in *Proc. IEEE Wireless Commun. Netw. Conf. (WCNC)*, Apr. 2019, pp. 1–6.

[20] C. Perfecto, J. Del Ser, and M. Bennis, "Millimeter-wave V2V communications: Distributed association and beam alignment," *IEEE J. Sel. Areas Commun.*, vol. 35, no. 9, pp. 2148–2162, Sep. 2017.

[21] Y. Wu, L. Yan, and X. Fang, "A low-latency content dissemination scheme for mmWave vehicular networks," *IEEE Internet Things J.*, vol. 6, no. 5, pp. 7921–7933, Oct. 2019.

[22] J. Gao, C. Zhong, X. Chen, H. Lin, and Z. Zhang, "Deep reinforcement learning for joint beamwidth and power optimization in mmWave systems," *IEEE Commun. Lett.*, vol. 24, no. 10, pp. 2201–2205, Oct. 2020.

[23] V. Va, X. Zhang, and R. W. Heath, Jr., "Beam switching for millimeter wave communication to support high speed trains," in *Proc. IEEE 82nd Veh. Technol. Conf. (VTC-Fall)*, Sep. 2015, pp. 1–5.

[24] V. Va, T. Shimizu, G. Bansal, and R. W. Heath, Jr., "Beam design for beam switching based millimeter wave vehicle-to-infrastructure communications," in *Proc. IEEE Int. Conf. Commun. (ICC)*, May 2016, pp. 1–6.

[25] I. Mavromatis, A. Tassi, R. J. Piechocki, and A. Nix, "Beam alignment for millimetre wave links with motion prediction of autonomous vehicles," *IET Semin. Dig.*, vol. 2017, no. 1, pp. 1–8, 2017.

[26] I. Mavromatis, A. Tassi, R. J. Piechocki, and A. Nix, "MmWave system for future ITS: A MAC-layer approach for V2X beam steering," in *Proc. IEEE 86th Veh. Technol. Conf. (VTC-Fall)*, Sep. 2017, pp. 1–6.

[27] R. Ismayilov, M. Kaneko, T. Hiraguri, and K. Nishimori, "Adaptive beam-frequency allocation algorithm with position uncertainty for millimeter-wave MIMO systems," in *Proc. IEEE 87th Veh. Technol. Conf. (VTC Spring)*, Jun. 2018, pp. 1–5.

[28] Y. Kang, H. Seo, and W. Choi, "Optimal receive beamwidth for time varying vehicular channels," in *Proc. IEEE Wireless Commun. Netw. Conf. (WCNC)*, May 2020, pp. 1–6.

[29] Y. Kang, H. Seo, and W. Choi, "When to realign the receive beam in high mobility V2X communications?" *IEEE Trans. Veh. Technol.*, vol. 69, no. 11, pp. 13180–13195, Nov. 2020, doi: 10.1109/TVT.2020.3021394.

[30] L.-H. Shen and K.-T. Feng, "Mobility-aware subband and beam resource allocation schemes for millimeter wave wireless networks," *IEEE Trans. Veh. Technol.*, vol. 69, no. 10, pp. 11893–11908, Oct. 2020, doi: 10.1109/TVT.2020.3006320.

[31] G. R. Muns, K. V. Mishra, C. B. Guerra, Y. C. Eldar, and K. R. Chowdhury, "Beam alignment and tracking for autonomous vehicular communication using IEEE 802.11ad-based radar," in *Proc. IEEE Conf. Comput. Commun. Workshops (INFOCOM WKSHPS)*, Apr. 2019, pp. 535–540.

[32] J. Kim, H. Kim, and S.-L. Kim, "Poster: Millimeter wave V2V communications with inaccurate location information," in *Proc. IEEE Veh. Netw. Conf. (VNC)*, Nov. 2017, pp. 35–36.

[33] *Study on Evaluation Methodology of New Vehicle-to-Everything (V2X) Use Cases for LTE and NR, Release 15*, 3GPP, document TR 37.885, Jun. 2019.

[34] W. Hao, F. Zhou, Z. Chu, P. Xiao, R. Tafazolli, and N. Al-Dhahir, "Beam alignment for MIMO-NOMA millimeter wave communication systems," in *Proc. IEEE Int. Conf. Commun. (ICC)*, May 2019, pp. 1–6.

[35] J. Wildman, P. H. J. Nardelli, M. Latva-aho, and S. Weber, "On the joint impact of beamwidth and orientation error on throughput in directional wireless Poisson networks," *IEEE Trans. Wireless Commun.*, vol. 13, no. 12, pp. 7072–7085, Dec. 2014.

[36] M. Torrent-Moreno, J. Mittag, P. Santi, and H. Hartenstein, "Vehicle-to-vehicle communication: Fair transmit power control for safety-critical information," *IEEE Trans. Veh. Technol.*, vol. 58, no. 7, pp. 3684–3703, Sep. 2009.

[37] J. Farrell and M. Barth, *The Global Positioning System and Inertial Navigation*. New York, NY, USA: McGraw-Hill, 1999.

[38] Y. Feng, J. Wang, D. He, and Y. Guan, "Beam design for V2V communications with inaccurate positioning based on millimeter wave," in *Proc. IEEE 90th Veh. Technol. Conf. (VTC-Fall)*, Sep. 2019, pp. 1–5.

[39] M. C. Grant and S. P. Boyd. *CVX: MATLAB Software for Disciplined Convex Programming, Version 2.2*. Accessed: Jan. 2020. [Online]. Available: http://www.cvxr.com/cvx/

[40] S. Boyd and L. Vandenberghe, *Convex Optimization* (The Edinburgh Building). Cambridge, U.K.: Cambridge Univ. Press, 2004.

[41] (Dec. 2019). *NVIDIA Introduces DRIVE AGX ORIN—Advanced, Software-Defined Platform for Autonomous Machines*. Nvidia. [Online]. Available: https://nvidianews.nvidia.com/news/nvidia-introduces-drive-agx-orin-advanced-software-defined-platform-for-autonomous-machines

[42] *Study on LTE-Based V2X Services, Release 14*, document TR 36.885, 3GPP, Jun. 2016.

[43] *Dedicated Short Range Communications (DSRC) Message Set Dictionary*, SAE Standard J2735, SAE Int., DSRC Committee, Nov. 2009.

[44] M. Amoozadeh, H. Deng, C.-N. Chuah, H. M. Zhang, and D. Ghosal, "Platoon management with cooperative adaptive cruise control enabled by VANET," *Veh. Commun.*, vol. 2, no. 2, pp. 110–123, Apr. 2015.

YIJIA FENG (Member, IEEE) received the B.Sc. degree from Southeast University, Nanjing, China, in 2015. She is currently pursuing the Ph.D. degree with Shanghai Jiao Tong University, Shanghai, China. Her research interests include V2X communication, UAV communication, and intelligent transportation systems.

DAZHI HE received the B.S. degree in electrical engineering from Tongji University, in 1999, and the Ph.D. degree from Shanghai Jiao Tong University, in 2009. He is currently an Associated Researcher with the Cooperative Media Network Innovation Center, Shanghai Jiao Tong University. His research interests include wireless transmission, heterogeneous networks, and cooperative communication.

YUNFENG GUAN received the Ph.D. degree from the Department of Electronics and Information Technology, Zhejiang University, Hangzhou, China, in 2003. Since 2003, he has been working with the Institute of Wireless Communication Technology, Shanghai Jiao Tong University. His research interests include wireless communications and digital TV.

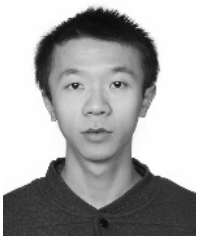

YIHANG HUANG received the bachelor's degree from the University of Electronic Science and Technology of China, in 2014. He is currently pursuing the Ph.D. degree in information and communication engineering with Shanghai Jiao Tong University. His research interests include digital signal processing and cooperative transmission by DTTB and cellular networks.

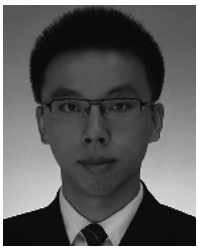

YIN XU (Member, IEEE) received the B.Sc. degree in information science and engineering from Southeast University, China, in 2009, and the master's and Ph.D. degrees in electronics engineering from Shanghai Jiao Tong University, in 2011 and 2015, respectively. He currently works as an Assistant Professor with Shanghai Jiao Tong University. He is active in participating in standardization progress in ATSC3.0 and 3GPP. He is interested in the theory and technology on converged broadcasting and broadband networks. His main research interests include channel coding, advanced bit-interleaved coded modulation, and other physical layer technologies in broadcasting and 5G.

ZHIYONG CHEN (Member, IEEE) received the Ph.D. degree from the School of Information and Communication Engineering, Beijing University of Posts and Telecommunications (BUPT), Beijing, China, in 2011. From 2009 to 2011, he was a Visiting Ph.D. Student with the Department of Electronic Engineering, University of Washington, Seattle, WA, USA. He is currently an Associate Professor with the Cooperative Medianet Innovation Center, Shanghai Jiao Tong University (SJTU), Shanghai, China. His research interests include mobile communications-computing-caching (3C) networks, mobile VR/AR delivery, and mobile AI systems. He was a recipient of the IEEE Asia-Pacific Outstanding Paper Award, in 2019. He has served as the Student Volunteer Chair for the IEEE ICC 2019, the Publicity Chair for the IEEE/CIC ICCC 2014, and a TPC member for major international conferences. He currently serves as an Associate Editor for IEEE Access.